BOUNDARY LAYER MODELS OF HYDROTHERMAL CIRCULATION ON EARTH AND MARS

A Thesis
Presented to
The Academic Faculty

by

Kathleen L. Craft

In Partial Fulfillment
Of the Requirements for the Degree
Master of Science in the
School of Earth and Atmospheric Sciences

Georgia Institute of Technology
December 2008

BOUNDARY LAYER MODELS OF HYDROTHERMAL CIRCULATION ON EARTH AND MARS

Approved by:

Dr. Robert Lowell, Advisor
School of Geosciences
Virginia Polytechnic Institute

Dr. Kurt Frankel
School of Earth and Atmospheric Sciences
Georgia Institute of Technology

Dr. Andrew Newman
School of Earth and Atmospheric Sciences
Georgia Institute of Technology

Date Approved: August 22, 2008

AKNOWLEDGMENTS

I would like to thank my adviser, Dr. Bob Lowell, for sharing his knowledge and lending guidance throughout my research. Also, I send many thanks to my fellow geophysics classmates at Georgia Tech including Kevin Chao, Jaime Convers, Grant Farmer, Abhijit Ghosh, Lujia Feng, Lei Liu, Chunquan Wu, and Peng Zhao who supported my work through their encouragement and the sharing of ideas and laughter. Many of the professors in Georgia Tech's Earth and Atmospheric Sciences department provided a strong foundation for which to build my research, and for this I am truly appreciative. In particular I would like to thank Dr. Carlos Cardelino, Dr. Kurt Frankel, Dr. Andrew Newman, Dr. Zhigang Peng, Dr. Wenyue Xu and also Dr. Leonid Germanovich in the Civil Engineering department. Additionally, Dr. Erin Kraal at Virginia Tech contributed to my Mars research and I want to thank her for her time and the knowledge she imparted to me.

I also give a big thank you to my parents for their continued support and loving encouragement throughout the years. Last, I would like to thank my wonderful husband. His optimistic outlook and ability to always make me smile carry me through and enable me to pursue and accomplish my goals.

This research was supported in part by NSF Grant OCE 0527208 to Robert P. Lowell.

TABLE OF CONTENTS

LIST OF TABLES

LIST OF FIGURES

LIST OF SYMBOLS

Variable	Definition
$c_{p,f}$	Specific heat of the fluid
$c_{p,m}$	Specific heat of the medium
f	Similarity variable for velocities
g	Gravitational acceleration
K	Permeability of the ground material
k	Thermal conductivity
P	Pressure acting on fluid
q_b	Heat flux
Ra	Raleigh number
T	Temperature
T_w	Temperature at the heated wall
T_∞	Temperature at infinite distance from heated wall
t	Time
u	Vertical velocity
u_∞	Vertical velocity at infinite distance from heated wall
$u_{1,2,3}$	u-substitution variables
V	Velocity
v	Horizontal velocity
v_∞	Horizontal velocity at infinite distance from heated wall
x	Vertical position
y	Horizontal position
α	Thermal diffusivity of the ground medium (country rock)
β	Thermal expansion coefficient of water
δ	Boundary layer thickness
Φ_m	Mass flux
η	Similarity variable for position
θ	Similarity variable for temperature
μ	Viscosity of the fluid
ψ	Stream function
ρ_f	Density of the fluid
ρ_∞	Density of the fluid at infinite distance from heated wall

SUMMARY

Continental and submarine hydrothermal systems are commonly found around the world. Similar systems that sustain water or other fluids are also likely to exist in planetary bodies throughout the solar system. The study of these systems is vital to the understanding of planetary heat transfer, chemical cycling, and biological processes; hence hydrothermal processes play a fundamental role in planetary evolution. On Mars, for example, hydrothermal processes may have caused the formation various geomorphic features such as valley networks, outflow channels, and gullies that have been attributed to the flow of water on the surface. Terrestrial submarine systems have been suggested as the locations of the first life on Earth and may, therefore, provide indications of where to find life on other planetary bodies. Investigations into hydrothermal systems will enable the understanding of planetary heat and chemical cycling and geomorphology formation processes and how they evolve over time.

In this thesis, three particular types of hydrothermal systems are investigated through the development of mathematical models: (1) terrestrial low-temperature diffuse flows at mid-oceanic ridges (MORs), (2) submarine near-axis convection on Earth, and (3) convection driven by magmatic intrusives on Mars. Key questions addressed concerning terrestrial systems include how much heat is released by focused high-temperature flow versus diffuse flow on MORs and how high-temperature flow transitions to low-temperature flow as the lithosphere ages. An important question investigated concerning

hydrothermal processes on Mars is the feasibility of hydrothermal systems as formation mechanisms for surface morphology.

Model set-ups for all systems include a two-dimensional space with a vertical, hot wall, maintained at constant temperature, located adjacent to a water-saturated porous medium at a lower temperature. By assuming that convection occurs vigorously and within a thin layer next to the hot wall, boundary layer theory is applicable. This theory enables the derivation of a general solution that is applied to the three different hydrothermal environments by using appropriate model parameters. The models provide estimates of the total heat and mass transfer rates in each scenario. Because the wall temperature is assumed to be constant, steady-state solutions are obtained. For simplicity, the boiling and phase separation are not considered and the fluid is assumed to remain in the liquid phase.

For seafloor terrestrial hydrothermal systems, the main variable is permeability, which is thought to vary over a range of from 10^{-14} to 10^{-10} m^2. Heat output results derived from the boundary layer model suggest that diffuse flow on MORs contributes 50% or less of heat output to the ridge system. This is at the low end of observations, suggesting that other models of diffuse flow need to be investigated before the boundary layer results can be confirmed. Boundary layer results also indicate that temperature distributions for near-axis systems are in reasonable agreement with those inferred from seismic tomographic studies of the oceanic crust and with other numerical models. For the near-axis model, results found that heat transfer in the hydrothermal boundary layer was greater than the

input from steady state generation of the oceanic crust by seafloor spreading. Therefore, this suggests that the size of the mushy zone is not in a steady-state.

For Martian hydrothermal systems, the gravitational acceleration of 3.7 m/s^2 is used and permeability is assumed to range between 10^{-14} to 10^{-8} m^2. Heat output and fluid flux calculations for Martian systems show that fluid outflow adjacent to a single intrusion is too small to generate observed Martian surface features in a reasonable length of time. Other considerations such as multiple dikes, the melting of subsurface ice, or hydrate dissociation may increase the fluid discharge resulting from hydrothermal heat transfer and promote the development of fluvial morphology on Mars.

CHAPTER 1. INTRODUCTION

Hydrothermal systems exist at many locations in the Earth in both continental and submarine environments. Analogous systems are likely to exist, or have previously existed on other planetary bodies where heat sources associated with volcanism, impacts, and tidal stresses generate large thermal gradients that can drive fluid circulation. These systems play an important role in planetary heat transfer. Moreover, they serve as energy resources and as agents for geochemical cycling and ore formation. Because hydrothermal systems have been linked to the origin of life on Earth (e.g., Baross and Hoffman, 1985), they may provide clues to the existence of life elsewhere in the solar system. Hydrothermal processes on Mars may also play or have played a role in shaping the surface. It is therefore of critical scientific importance to understand hydrothermal processes not only on Earth but also on other planetary bodies.

Hydrothermal systems form when a water-saturated permeable medium encounters a heat source that transfers heat to the water and drives fluid circulation. The circulation results from hot, low-density fluid rising close to the heat source and colder water, which moves in to replace the hot water, also then increases in temperature and rises. As long as the heat source is maintained and any discharged fluid is replenished, circulation will continue. Circulating hydrothermal fluid will also react chemically with the rock medium and can discharge minerals dissolved from the subsurface.

This thesis develops mathematical models to elucidate certain types of submarine hydrothermal processes on Earth and also investigates possible similar hydrothermal processes on Mars.

1.1 Characteristics of terrestrial submarine and Martian hydrothermal systems

1.1.1 Submarine systems on Earth

Submarine hydrothermal systems on Earth form when seawater enters into young and permeable oceanic crust of ages up to 65 ± 10 Ma (Stein and Stein, 1994) where temperature gradients within the crust cause heat exchanges with the seawater and induce convection and circulation. These systems contribute significantly to Earth's heat transfer by means of both high-temperature focused flow near oceanic spreading centers and low-temperature diffuse flows, particularly in older lithosphere away from mid-ocean ridge axes. According to heat flow model estimates compiled by Elderfield and Schultz (1996), about 25% of the total global heat flux occurs from hydrothermal flow in crust younger than ~ 65 Ma. Stein and Stein (1994) estimate that hydrothermal flow accounts for 34% of the global oceanic heat flux and that ~30% of oceanic hydrothermal flow occurs within crust younger than 1 Ma. According to this estimate, the majority (~70%) of hydrothermal heat flow occurs off-axis. Often, low-temperature diffuse flows occur adjacent to the high-temperature focused venting; however, the fractionation of the contributions by high-temperature focused and to oceanic hydrothermal heat flux is not exactly known.

Oceanic hydrothermal systems also play a major role in controlling seawater chemistry (e.g., Wolery and Sleep, 1976; Edmond, 1982; Elderfield and Schultz, 1996) and potentially harbored the first life on Earth (e.g., Baross and Hoffman, 1985). Evidence of the effect of hydrothermal circulation on seawater chemistry first became apparent in data gathered from hydrothermal venting at the Galapagos Spreading Center (Edmond et al., 1979), where vent fluids were enriched in rubidium, lithium, potassium, silica and barium and were depleted in magnesium and sulfate. Edmond et al. (1979) thus suggested that hydrothermal circulation was a significant chemical cycling mechanism. Considering these and other ridge system chemistries, Baross and Hoffman (1985) argued that hydrothermal systems contained all physical and chemical components required for life to originate including: (1) a continuous and concentrated source of energy; (2) diverse physical and chemical conditions for the sequential evolution from chemical to ecosystem states; (3) a short time requirement for biology to evolve given the geologically small time interval between oceans forming and microorganisms appearing in the fossil record; and (4) vital trace elements for nitrogen-cycling reactions.

In order to improve the understanding of oceanic hydrothermal system processes and their effect on Earth's heat budget, this investigation focuses on hydrothermal circulation at both mid-oceanic ridges (MOR) axes and in the transition zone between high-temperature ridge-axis systems and the low-temperature off-axis systems that predominate in lithosphere greater than several million years old. Those hydrothermal systems occurring in the transition area are termed "near-axis" systems. Together, near-axis and MOR systems, although small in relative area, are estimated to produce about

10% of the ocean's hydrothermal heat flux, making them a significant contributor to the global oceanic heat and chemical budgets (Stein and Stein, 1994).

1.1.1.1 Mid-oceanic ridge systems

Hydrothermal flow at mid-oceanic ridges is characterized by high-temperature focused flow. The hot (~350° to 400°C), metal-laden hydrothermal fluid discharges at the seafloor through small vent orifices or chimneys and mixes with the cold seawater, causing sulfide rich, dark-colored precipitates to form (Spiess et al., 1980). Hence, they are often referred to as "black smokers." These vents were first discovered in the late 1970s (Spiess et al., 1980) and since that time, about 150 black smoker vent fields have been located during field expeditions and a similar number of sites have been inferred indirectly from thermal or chemical anomalies in the water column above active spreading centers (Baker and German, 2004).

In addition to high-temperature focused flow, low-temperature diffuse flows ($T < 100°C$) often occur near high-temperature vents at MORs (e.g., Schultz et al., 1992; Edmond et al., 1995; James and Elderfield, 1996; Humphris and Tivey, 2000; Von Damm and Lilley, 2004; Ramondenc et al., 2006; Scheirer et al., 2006). The origin of the low-temperature flow is not well understood and may result from high-temperature flow transferring heat and inducing convection in the shallow crust (e.g., Lowell et al, 2003; 2007), or from high-temperature flow entering shallow crust from below and mixing with low-temperature seawater (Germanovich et al., 2000; 2001; Ramondenc et al., 2008). If high-temperature and low-temperature fluids mix and result in fluid with a temperature greater

than 150°C, anhydrite can precipitate and form a relatively impermeable vertical wall (e.g., Lowell et al., 2003), resulting in a barrier between the high- and low-temperature circulation regimes. The high-temperature fluid would then transfer heat through the wall by conduction induce circulation in the adjacent crustal rocks.

Measurements of heat flow at MORs thus far have not conclusively determined the fraction of heat attributed to high-temperature flow and to low-temperature diffuse flow. Veirs et al. (2006) estimated diffuse flow contributed 50% of the heat flow measured at the Main Endeavour Vent Field on the Juan de Fuca Ridge, while Schultz et al. (1992) estimated a value of 90%. Rona and Trivett (1992) estimate 90% diffuse flow at another medium-rate spreading center, the Axial Volcano on the Juan de Fuca Ridge, and Ramondenc et al. (2006) estimated the diffuse flow contribution at 9°50′ N on the East Pacific Rise at greater than 90%. The differences in these measurements can not be explained by the different rates of sea floor spreading at the two separate MOR systems as these are instantaneous measurements and the hydrothermal systems are likely to be short-lived relative to seafloor spreading rates. Also, the data collected by Veirs et al. (2006) and Schultz et al. (1992) are for the same system, but they used different measurement techniques. In an effort to understand the fractionation of high- and low-temperature flows, this thesis analyzes the possible cases of: (1) a high-temperature flow inducing convection of seawater in the shallow crust and (2) a system containing a precipitate layer that transfers heat from the adjacent high-temperature flow on one side to the cold seawater just below the seafloor on the other side. Because heat transfer from

a hot vertical boundary drives the flows, they can be described in terms of convection near a hot vertical wall (section 1.2).

1.1.1.2 Near-axis systems

Hydrothermal circulation has been inferred to occur in crustal ages up to ~ 65 Ma (Stein and Stein, 1994) based on the difference between observed conductive heat flow and models of cooling lithosphere. The off-axis circulation is generally thought to occur at low temperature because of the absence of magmatic heat sources (e.g., Wolery and Sleep, 1976). Between these off-axis areas of low-temperature diffuse flow and the high-temperature flow on the ridges, a transition region exists where near-axis hydrothermal systems are located. This environment is relatively unexplored, but Haymon et al. (2005) may have detected evidence of a near-axis system about 5 km east of the East Pacific Rise on 0.1 Ma crust. The lack of Cu and Zn minerals in the vent fluids there indicated a discharge temperature below 140°C (Benjamin, 2004).

How the transfer from a ridge-crest hydrothermal system to off-axis hydrothermal flow occurs is not completely understood. Seismic data collected by Dunn et al. (2000) at the East Pacific Rise using ocean bottom seismographs enabled calculation of thermal contours describing the ridge and near-axis regions (Figure 1.1). As shown in Figure 1.1, the seismic data suggested that compact temperature contours lie against a "hot wall", denoting the boundary between partially molten and solidified crust in the near-axis region. Such a thermal structure appears similar to that expected for induced flow near a

hot boundary and can be investigated using techniques described in section 1.2 and formulated in Chapter 2.

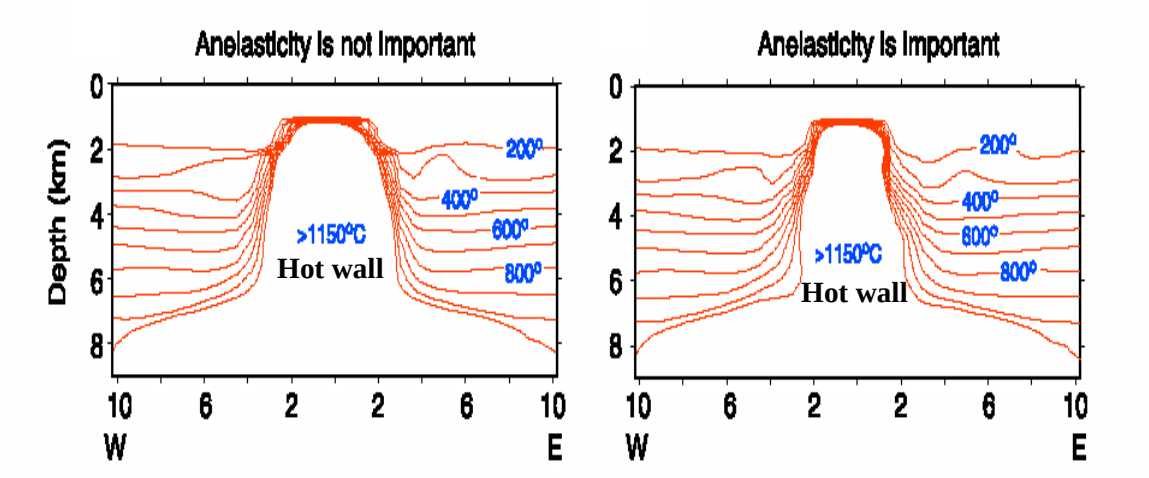

Figure 1.1: Isotherms interpreted from seismic data collected by Dunn et al. (2000) at the East Pacific Rise. The vertical high-temperature area at > 1150°C acts as a "hot wall" that transfers heat to the adjacent medium. For both cases shown, the isotherms are compact and vertical.

1.1.2 Martian systems

Hydrothermal systems similar to those on Earth may also exist or have previously existed on Mars as suggested by the volcanic and fluid flow-like surface morphology (Baker and Milton, 1974; Carr, 1979; Baker, 2001). These systems may answer questions concerning how valleys, gullies and other surface morphology were formed early in the geologic history of Mars as well as how some recent morphological features form (e.g. NASA, 2006; Malin and Edgett, 2000). For example, Figure 1.2 shows images taken by the Mars Global Surveyor of the same crater at two separate times. In the second picture, a white

deposit exists that was not present in the earlier photo. Due to the characteristics of the deposit, the material is suggested to have resulted from flowing water (NASA, 2006).

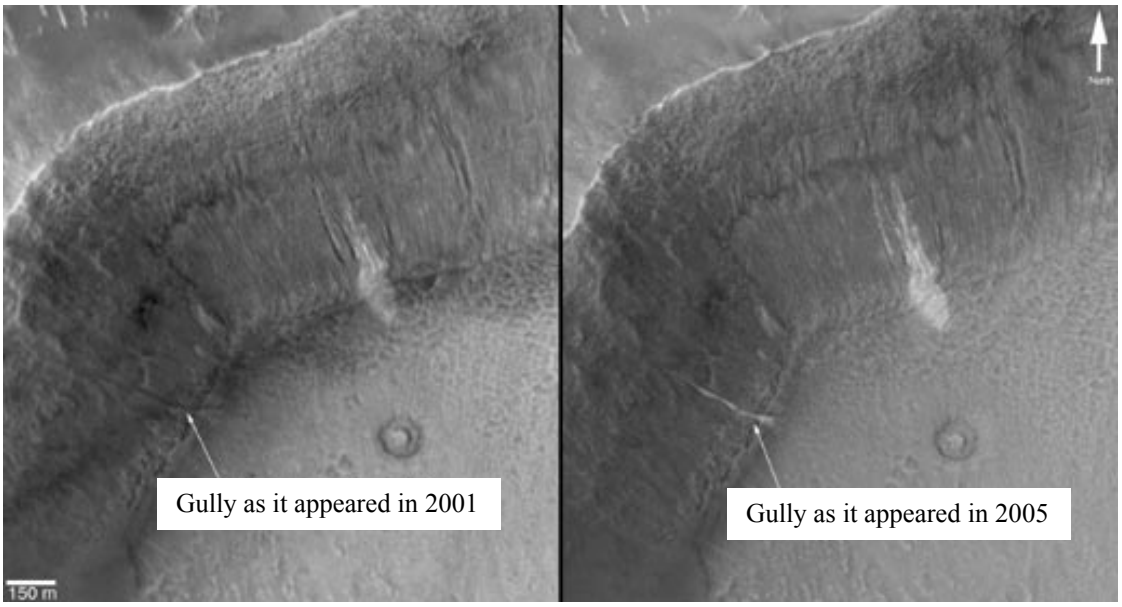

Figure 1.2: Images taken by the Mars Global Surveyor spacecraft of a crater on Mars. The right image shows a white deposit not present in the left image, which was taken 4 years earlier (NASA, 2006).

Hydrothermal systems driven by a magmatic intrusion on Mars may have heated nearby ground water that rose buoyantly to the surface, where it discharged and carved valleys and other fluvial surface morphology. Although rainfall may have formed the morphology on Mars if the Martian atmosphere was denser in the past, as suggested by Cloy (1984) and Pollack et al. (1987), observations of isolated valley systems and of sapping characteristics instead of runoff attributes argue against rainfall as the only formation mechanism (Brakenridge et al., 1985; Gulick, 2001). Also, recent findings by the NASA probe, Phoenix, confirm that there is currently water ice beneath the surface of Mars at the poles (NASA, 2008). This supports the possibility that frozen and/or liquid

water may exist below the surface at lower latitudes as a fluid source for the hydrothermal systems (eg., Squyres et al., 1987; McKenzie and Nimmo, 1999; Ogawa et al., 2003).

Numerical models performed on Martian hydrothermal systems to determine if hydrothermal fluid has and/or can currently alter the surface include: investigation of a system driven by a magma intrusion by Gulick (1998); a study on an impact induced hydrothermal system by Rathbun and Squyres (2002); and an analysis on shallow sills and surface magma flows as mechanisms for melting subsurface ice and releasing the fluid by Squyres et al. (1987). This study focused on magma driven hydrothermal systems and quantified the heat and fluid output for a range of possible Martian regolith permeabilities. The lower bound for permeability considers minimum fluid flow in basaltic mediums, while the highest permeability used was chosen as a reasonable value for an intact basaltic regolith. As discussed in section 1.2, Martian hydrothermal systems were analyzed in the context of fluid flow adjacent to a hot vertical boundary and hence the methodology was similar to hydrothermal models for terrestrial marine systems.

By investigating hydrothermal systems on other planets, much can be learned about terrestrial systems as well. Although certain parameters differ such as gravity and permeability, other attributes including the similar basaltic mediums and the consistency of the physics of heat transfer and induced fluid circulation for all environments suggest the systems should behave similarly. Additionally, one system may provide insight into an aspect not easily observed at the other system. Just as Earth systems contain all the

necessities for life, so too may Martian hydrothermal systems harbor microorganisms. Hydrothermal circulation and convection causes mixing of minerals and elements in a warm environment conducive to how life is thought to have evolved on Earth (Baross and Hoffman, 1985).

1.2 Convection near heated vertical walls

In order to gain a greater understanding of hydrothermal system behavior, hydrothermal circulation driven by lateral temperature gradients resulting from a vertical, high-temperature wall was modeled for: (1) terrestrial high-temperature focused and low-temperature diffuse flows on mid-oceanic ridges, (2) submarine near-axis convection, and (3) convection driven by Martian intrusives. Assuming that vigorous convection occurs in these systems, an appropriate way to consider this is to apply the boundary layer theory (Cheng and Minkowycz, 1977). This theory approximates the conditions of hydrothermal systems by considering heat transfer from a vertical, heated wall to a porous medium saturated with water at a lower temperature. In this simplified model, the hot vertical wall represents a high-temperature focused flow or a heated precipitate boundary in a MOR system, the partially molten boundary in the near-axis submarine system, and a magma intrusion for a Martian system. Also, the boundary layer theory assumes that convection takes place within a relatively thin layer next to the vertical wall and achieves a steady-state solution. Chapter 2 of this thesis sets up the basic mathematical formulation of boundary layer theory and derives the basic steady-state, dimensionless solutions.

Chapter 3 describes the application of the boundary layer theory to submarine hydrothermal systems. The theory was used to investigate: (a) the relative importance of high-temperature focused and low-temperature induced diffuse flows on mid-oceanic ridges and (b) the heat transfer associated with near-axis circulation at the edge of the partially molten zone in the lower crust. A range in permeability was used for the porous medium adjacent to the flows and the heated wall height was varied to determine the sensitivity of the heat and mass flux results to these parameters. Results from the models indicate the fractionation of heat transfer between the high-temperature focused flows and the low-temperature diffuse flows for a given system. Near-axis convection was also modeled using the boundary layer theory and heat and mass fluxes were determined.

Chapter 4 explains the application of this modeling approach to Martian hydrothermal systems. Heat transfer and mass flow were calculated using the boundary layer theory and these calculations and results are explained in detail. To allow for uncertainties of the Martian regolith, a range in permeability of was considered and the depth of the magma chamber (wall height) was varied to determine the sensitivity of the heat and mass fluxes to these parameters. Additionally, the mass transfer results were compared to the flux amounts required to produce surface geomorphology on Mars as predicted by other models. In this way, it was determined whether or not hydrothermal systems could produce an adequate amount of fluid over time to form Martian morphology.

Finally, Chapter 5 revisits the motivation for this research and summarizes the principle results. An overall view is given of the terrestrial submarine and Martian hydrothermal

systems' heat and mass flux results and relates how these contribute to the knowledge of the systems as a whole. Lastly, possible directions for future work are discussed.

CHAPTER 2. METHODOLOGY

2.1 Introduction

The investigation performed here studies the particular hydrothermal systems in which fluid flow is driven by heat transfer adjacent to a hot, vertical boundary. By simplifying the system, considerable insight can be gained without performing complicated numerical calculations. A heated vertical wall, maintained at a certain constant temperature, represents the system's thermal source and a water-saturated porous medium sits adjacent to the heated wall. Thermal convection processes can then be studied as lateral temperature gradients transfer heat from the wall to the saturated medium. A range of permeabilities extending over several orders of magnitude is considered for the various systems and the thermal properties of the silicate medium are assumed to remain constant since variations in these properties are small compared to the range of permeability values considered.

By making the assumption that convection is vigorous and occurs within a thin layer, the boundary layer theory, as described by Cheng and Minkowycz (1977) and Bejan (1984), can be used to derive a general solution. The boundary layer theory takes the governing, non-linear differential equations for a hydrothermal system and reconfigures them as a set of coupled ordinary differential equations (ODEs). Standard numerical integration techniques can then be used to solve the ODEs and enable calculations of velocities and temperatures within the boundary layer and the layer's thickness. Additionally, integration of the temperature and velocity profiles over the thickness of the boundary layer results in heat and mass fluxes for different vertical locations within the

hydrothermal system. This chapter describes the methods used to solve the boundary layer model for hydrothermal systems and the calculations performed to find heat and mass flux and boundary layer thickness.

Figure 2.1 depicts the two-dimensional model and boundary conditions for a hydrothermal system. Horizontal position within the model is denoted by y, and vertical position is given by x. The vertical, impermeable, heated wall at constant temperature, T_w, conducts heat through to the fluid saturated medium initially at temperature equal to 4°C. T_w varies depending on the conditions of the hydrothermal system in which the wall is emplaced. Other parameters noted in Figure 2.1 include gravity, g, and the horizontal and vertical fluid velocities infinitely far from the heated wall, v_∞ and u_∞ respectfully, which are set to zero. Additionally, there is no heat flux across the bottom horizontal boundary ($q_b = 0$). Definition of variables and parameters used in this thesis are given in the List of Symbols on p. ix.

As heat is transferred by conduction from the hot wall to the adjacent fluid its density decreases and the fluid flows upward. The fluid that moved upwards leaves a vacancy that the cooler water further from the wall moves in to fill. If the wall temperature is fixed, a steady-state circulation will occur. For the boundary layer model, an assumption is made that outside of the boundary layer there is little change in temperature and velocity from the initial values. The change in velocity and temperature across the boundary layer thickness are shown schematically in Figure 2.1 by the profiles drawn in purple (velocity) and orange (temperature).

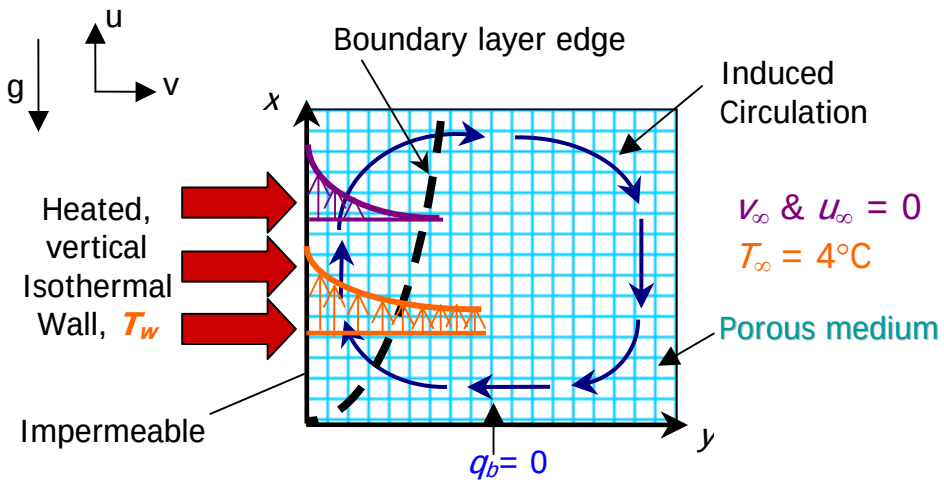

Figure 2.1: Sketch of model area and the boundary conditions for the 2 dimensional boundary layer flow model. Buoyant fluid ascends through a narrow region near the vertical hot wall, transferring heat towards the top of the model. Variable definitions are listed in the List of Symbols p. ix.

2.2 Boundary Layer Modeling

Modeling begins by determining the governing equations of the hydrothermal system. These include the conservation of mass (equation (2.1)), Darcy's law (conservation of momentum) (equations (2.2) and (2.3)), conservation of energy (equation (2.4)), and density dependence on temperature (equation (2.5)) (Bejan, 1984; Cheng and Minkowycz, 1977) modified for a two-dimensional system:

$$\frac{\partial u}{\partial x}+\frac{\partial v}{\partial y}=0 \tag{2.1}$$

$$u=(-K/\mu)(\frac{\partial P}{\partial x}+\rho_f g) \tag{2.2}$$

$$v=(-K/\mu)\frac{\partial P}{\partial y} \tag{2.3}$$

$$c_{p,f}\rho_f v.\nabla T = k\nabla^2 T \tag{2.4}$$

$$\rho_f = \rho_\infty\left[1-\beta(T-T_\infty)\right] \tag{2.5}$$

Where the variables are defined as: *v, u*: horizontal and vertical velocities of the fluid respectively; *y, x*: horizontal and vertical position respectively; $c_{p,f}$: specific heat of fluid; *g*: gravity; *K*: permeability; *k*: thermal conductivity; *P*: pressure; *T*: temperature; T_∞: temperature infinitely far from hot wall; β: thermal expansion coefficient of water; μ: fluid viscosity; ρ_f: fluid density; ρ_∞: density infinitely far from hot wall. Boundary conditions are then set for the system. Equations (2.6) and (2.7) state the velocity and temperature conditions along the heated vertical wall. Equations (2.8) and (2.9) describe the velocity and temperature conditions at an infinite distance from the heated vertical wall.

$$y = 0, \qquad v = 0 \tag{2.6}$$

$$y = 0, \qquad T = T_w \tag{2.7}$$

$$y \text{ -> } \infty, \qquad u = 0 \tag{2.8}$$

$$y \text{ -> } \infty, \qquad T = T_\infty \tag{2.9}$$

The horizontal velocity, *v*, and vertical velocity, *u*, are defined in terms of the stream function ψ by:

$$v = -\frac{\delta\psi}{\delta x} \tag{2.10}$$

$$u = \frac{\delta \psi}{\delta y} \tag{2.11}$$

2.3 Similarity Solution

Given the aforementioned assumptions and boundary conditions, the hydrothermal system's non-linear governing equations are simplified and converted into ordinary differential equations using a set of dimensionless similarity variables:

$$\eta = Ra_x^{1/2}(y/x) \tag{2.12}$$

$$f(\eta) = \frac{\psi}{\alpha Ra_x^{1/2}} \tag{2.13}$$

$$\theta(\eta) = \frac{(T - T_\infty)}{(T_w - T_\infty)} \tag{2.14}$$

where the Raleigh number, Ra_x is defined as:

$$Ra_x = \frac{\rho_\infty g \beta K (T_w - T_\infty) x}{\mu \alpha} \tag{2.15}$$

Substituting the similarity variables (2.12), (2.13), and (2.14), into the governing equations (2.1), (2.2), (2.3) and (2.4), results in two ordinary differential equations:

$$f'' - \theta' = 0 \tag{2.16}$$

$$\theta'' + \frac{1}{2} f\theta' = 0 \tag{2.17}$$

(Cheng and Minkowycz, 1977). Further simplification is achieved by integrating equation (2.16) and applying the boundary conditions to obtain equation (2.18).

$$f' = \theta \tag{2.18}$$

Finally, equation (2.18) is differentiated twice and substituted into equation (2.17) to arrive at one higher order differential equation:

$$f''' + \frac{1}{2} ff'' = 0 \tag{2.19}$$

2.4 U-Substitution

U-substitution is then used to solve the higher order differential equation (personal communication Cardelino, 2007). First, equation (2.19) is rewritten as a system of *u* variables where:

$$f = u_1 \tag{2.20}$$

$$\frac{df}{d\eta} = \frac{du_1}{d\eta} = u_2 = u_1' \tag{2.21}$$

$$\frac{d^2 f}{d\eta^2} = \frac{du_2}{d\eta} = u_3 = u_2' \tag{2.22}$$

$$\frac{d^3 f}{d\eta^3} = \frac{du_3}{d\eta} = u_3' = -\frac{1}{2} f f'' = -\frac{1}{2} u_1 u_3 \tag{2.23}$$

Next the initial conditions (equations (2.6) and (2.7)) are converted to the *u* system:

When $y = 0$, $v = 0$ => when $\eta = 0$, $f = u_1 = 0$.

When $y = 0$, $T = T_w$ => when $\eta = 0$, $\theta = f' = u_2 = 1$

The third required initial condition, when $\eta = 0$, $f'' = u_3 = ?$ is not known. However, it is known that when η approaches infinity, $f' = u_2$ approaches zero. Therefore, the value for $u_3(0)$ is found by trying high and low values for $u_3(0)$ and narrowing to the correct value that causes u_2 to go to zero as $\eta \to \infty$. A *Matlab*® program was written to solve for $\eta = 0$, $f'' = u_3 = ?$ and for the values of $f(\eta)$, $f'(\eta)$, and $f''(\eta)$ (Appendix A). Results found that $u_3 = -0.444$ when $\eta = 0$. Figures 2.2, 2.3, and 2.4 show the similarity solutions for $f(\eta)$, $f'(\eta)$, and $f''(\eta)$.

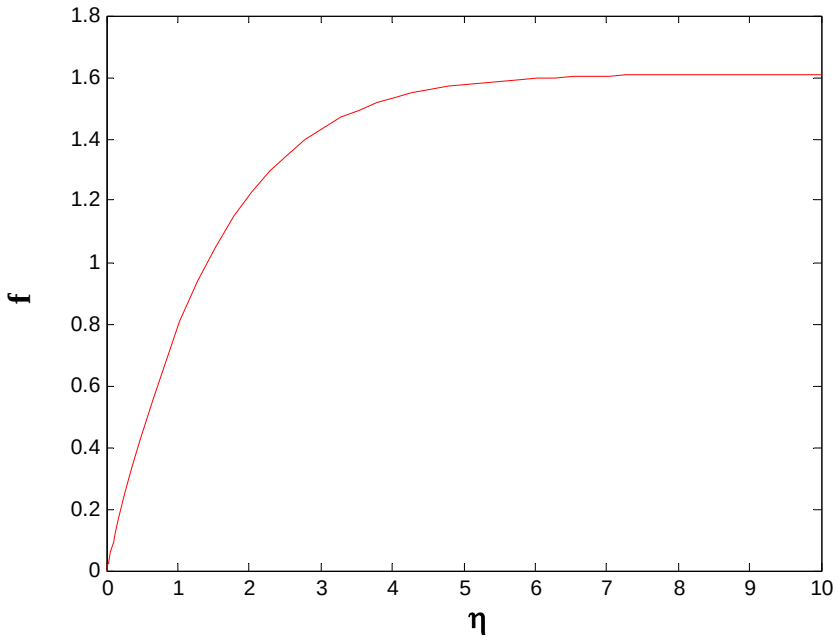

Figure 2.2: Similarity solution for f(η).

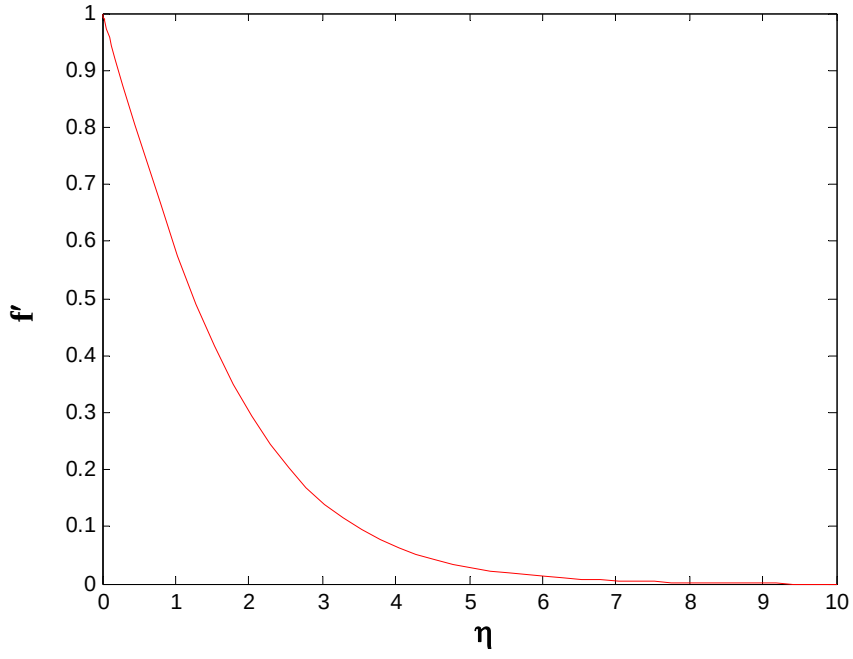

Figure 2.3: Similarity solution for f′(η)

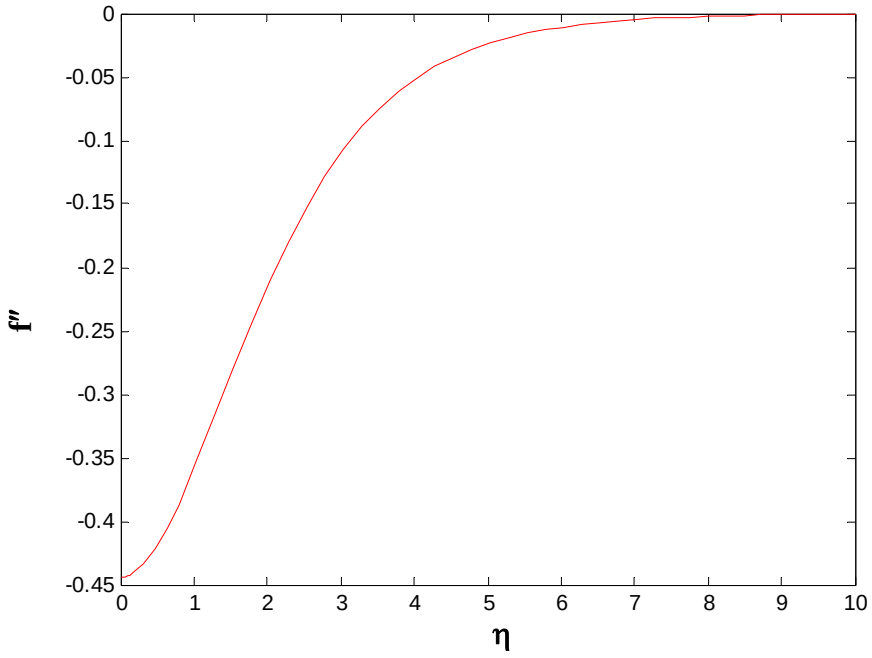

Figure 2.4: Similarity solution for f″(η)

Velocities and temperatures are then calculated by combining equations (2.10), (2.11), (2.12), (2.13), (2.14) and (2.15) and inserting values from the solutions for $f(\eta)$, $f'(\eta)$, and $f''(\eta)$ (Cheng and Minkowycz, 1977):

$$u = [\rho_\infty g\beta(T_w - T_\infty)K/\mu]f'(\eta) \tag{2.24}$$

$$v = 0.5[\alpha\rho_\infty g\beta K(T_w - T_\infty)/\mu x]^{1/2}[\eta f'(\eta) - f(\eta)] \tag{2.25}$$

$$T = f'(\eta)(T_w - T_\infty) + T_\infty \tag{2.26}$$

Fortran programs (Appendix A) were then written to solve for the velocities and temperatures for specified Martian and terrestrial parameters. Additionally, the boundary layer thickness (i.e. the thickness of the increased fluid temperature and velocity zone)

can be calculated by assuming that the edge of the boundary is where $\theta = 0.01$. Then, by determining the value of η at $\theta = f' = 0.01$ (hereafter referred to as, η_δ) from the solution for Figure 2.3, and rearranging equation (2.12), the boundary layer thickness can be obtained:

$$\delta = y = \frac{\eta_\delta}{(Ra_x)^{1/2}} \tag{2.27}$$

These solutions are used in subsequent investigations pertaining to hydrothermal systems at terrestrial, deep sea, and mid-ocean ridge locations as well as within Martian subsurface regolith near locations of possible magmatic intrusions. Heat transfer and fluid flow that these systems can produce are calculated and discussed in the following chapters.

CHAPTER 3. BOUNDARY LAYER MODELS IN TERRESTRIAL OCEANIC CRUST

3.1 Introduction

As discussed in Chapter 1, this thesis investigates two key, and poorly understood, issues concerning hydrothermal circulation within the oceanic crust. One issue regards the fractionation of heat output between focused and diffuse flows at oceanic ridge axes. The second issue concerns the transition from high-temperature flow to low-temperature flow as the lithosphere ages. Few studies have modeled the convection in this "near-axis" region.

At mid-ocean ridges, heat output measurements collected at individual high-temperature vents and plumes do not correspond with estimates based on upper water column data, which tend to be greater (Ramondenc et al., 2006; Baker, 2007). High-temperature flow must therefore not be the only contributor to the heat-output in these areas. Low-temperature diffuse flow is often observed to occur near the high-temperature focused flow vents and is believed to add a sizable amount to the heat flux measured in upper water column. A few examples of high-temperature vents adjacent to low-temperature diffuse flow include the Endeavour segment on the Juan de Fuca Ridge (Schultz et al., 1992), the Mid-Atlantic Ridge Trans Atlantic GeoTraverse (TAG) vent field (Edmond et al., 1995; Humphris and Tivey, 2000; James and Elderfield, 1996), the East Pacific Rise at 9°50′N (Ramondenc et al., 2006) and the ASHES vent field in the caldera of the Axial Volcano on the Juan de Fuca Ridge (Rona and Trivett, 1992). Although diffuse flow is known to contribute to the heat output, the fractionation between the high-temperature

and low-temperature flows is unknown. Previous estimates for diffuse flow heat flux range from 90% or more (e.g., Schultz et al., 1992; Rona and Trivett, 1992; Ramondenc et al., 2006) to closer to 50% (Veirs et al., 2006).

Relatively little hydrothermal modeling has been performed to address the relationship between focused and diffuse flow. Pascoe and Cann (1995) studied hydrothermal circulation and mixing between the deeper, high-temperature flow and the cooler, shallow oceanic crust fluid using a two-limb single pass model. For this model, one limb refers to the circulation deep in the crust, while the second limb circulation occurs in the layer 2A extrusive section of the crust, with the two limbs coinciding in a mixing region (e.g. Lowell et al., 2003; Ramondenc et al., 2008) as shown in Figure 3.1.

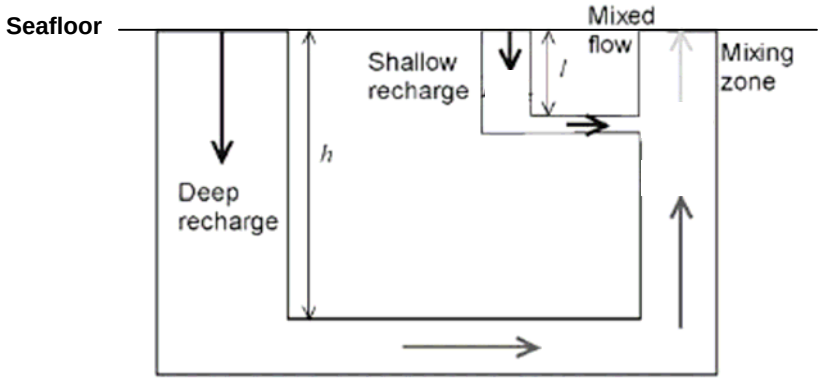

Figure 3.1: Two-limb, single-pass model modified from Lowell et al. (2003). Depicts the shallow and deep circulation limbs.

Pascoe and Cann (1995) suggested that mineral precipitation may cause an initially spread out flow to become focused as the precipitation builds up and decreases the

permeability of the crustal layer. Anhydrite precipitate has been observed at hydrothermal mounds (e.g., Tivey et al., 1998; Fouquet et al., 1998) and is believed to occur as a result of hot fluid discharge and cold seawater mixing and forming a fluid at a temperature greater than 150°C (Lowell et al., 2003).

Lowell et al. (2003) extended the suggestion of Pascoe and Cann through a model that investigated anhydrite precipitation in hydrothermal systems and quantified the conditions required to form a precipitate layer. Lowell et al.'s (2003) model showed that if the mixing zone permeability was greater than 10^{-12} m^2 but less than or equal to the permeability of the deep part of the discharge zone, then a focused black smoker would develop on the order of years. Otherwise, diffuse, low-temperature flow would occur. Lowell et al. (2003) also suggested that a 1- to 100-m-thick, relatively impermeable, vertical anhydrite layer could form where high-temperature flow mixed with low-temperature seawater in the shallow crust. This layer would then become a lower-temperature "hot" wall that may induce circulation in the colder seawater outside of it. Lowell et al. (2007) performed numerical simulations in a single-pass model of a MOR hydrothermal system and investigated the effects of a low-permeability vertical layer within the layer 2A extrusives. Their results showed that such a layer acts to segregate the high-temperature and low-temperature flows and causes a secondary region of high heat output on the cold side of the layer.

Ramondenc et al. (2008) also investigated the possibility of coupling between focused and diffuse flows and earthquakes. Their study modeled the flows using a two-branch

single-pass approximation taking into account both shallow (~100 m) and deep (~1.5 km) circulation and how the flows were affected by fracturing and other permeability changing events. Results of the Ramondenc et al. (2008) study showed that thermal perturbations at depth must affect the boundary layers both on the seafloor and where the high-temperature fluid mixes with the seawater in order to induce noticeable surface thermal changes. These results indicate a connection between focused and diffuse flows.

In addition to ridge-axis hydrothermal systems, near-axis systems may also play an important role in Earth's heat, fluid, and chemical transfer. Not much is known about this region, which falls between the ridge axis with high-temperature discharge and the off-axis region where hydrothermal discharge occurs at low temperature. Analysis of near-axis systems will allow insight into how this heat flow transition occurs. The approach taken in this investigation stemmed from examining the seismic data obtained by Dunn et al. (2000) at the East Pacific Rise (EPR). Thermal contours interpreted from the seismic data (Figure 1.1) are similar in form to that of boundary layer flow (Figure 2.1). The seismic data also help constrain the vertical wall height and temperature. These parameters and the study approach are discussed further in section 3.2.

To gain a greater understanding of these two key problems concerning oceanic hydrothermal system behavior, hydrothermal circulation driven by heat transfer from a vertical, high-temperature wall was modeled as presented in Chapter 2. The following section details the methodology utilized to complete the analyses.

3.2 Models

Oceanic crust is normally divided into three layers with the uppermost layer, layer 1, consisting of sediments, layer 2 containing basalt, and layer 3 made of gabbro. Layer 2 is further separated into sub-layers, yet the divisions are not universally agreed upon. Figure 3.2 shows a general schematic of the various layers taken from Bratt and Purdy (1984).

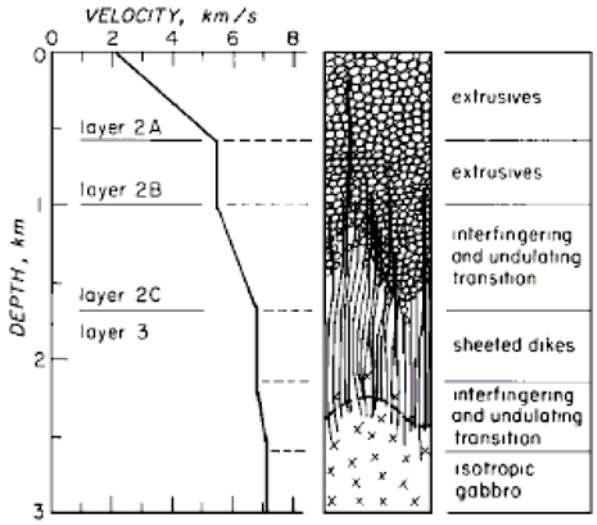

Figure 3.2: Schematic of subsurface oceanic layers. Taken from Bratt and Purdy (1984).

Some authors divide the layer into three parts; layers 2A, 2B and 2C. Fowler (2005) describes the layers: 2A represents the uppermost porous extrusives, with a depth of about 600 m and an increase in seismic velocity from 2 km/s to about 5 km/s; layer 2B contains less porous extrusives at an additional 400 m depth, and little change in seismic velocity; and the lowest layer, 2C, consists of sheeted dikes another ~600m deep with an increase of seismic velocity to about 6.2 km/s. Other authors divide layer 2 into two layers, 2A and 2B, where 2A includes extrusives and 2B contains sheeted dikes (e.g.,

Francheteau et al., 1992; Christeson et al., 1992; Harding et al., 1993; Kappus et al., 1995). According to Kappus et al. (1995) the velocity changes from 2.45 km/s ± 3% along the seafloor to 5 km/s ± 10 % at the top of layer 2B. The depth of layer 2A basalts ranges from 100 - 200 m at the ridge axis to 250 - 600 m within 1 to 4 km of the ridge (Harding et al., 1993; Vera and Diebold, 1994). Typically, the distinguishing factor between layers 2A and 2B is the sudden change in seismic velocity from ~ 2.5 to ~5 km/s. However, recent data indicate that the change in seismic velocity may be due to mineral precipitation causing porosity change rather than lithologic change (Christeson et al., 2007).

The high-temperature flows that occur at MORs are assumed to discharge through deep-seated high-permeability zones that act as quasi-vertical boundaries and induce circulation of seawater in the layer 2A basalts that comprise the uppermost portion of the crust since layer 1 sediments do not exist at mid-ocean ridges. Figure 3.3 depicts a hydrothermal system with a high-temperature discharge zone causing fluid circulation and boundary layer formation. Using this model, the focused high-temperature discharge flow was treated as a vertical, heated wall next to a permeable 2A basalt layer. These flows are observed to occur between 300° and 400°C (Spiess, 1980; Von Damm et al., 1995; Von Damm, 1990).

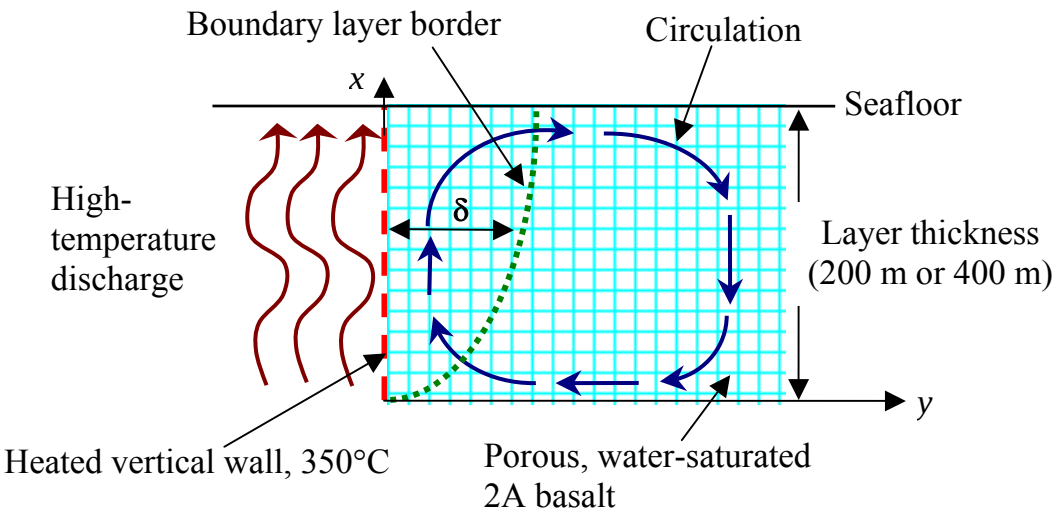

Figure 3.3: Sketch of mid-ocean ridge high-temperature hydrothermal system. The high-temperature discharge warms adjacent water in the 2A basalt layer and causes circulation. A boundary layer is formed close to the heated wall. Symbols are defined in the List of Symbols on p. ix.

For this model, the wall temperature was set to a representative black smoker temperature of 350°C and the resulting temperature and velocity profiles were calculated for layer 2A thicknesses of 200 m and 400 m. The 2A layers can be thicker further from the axis, however for this analysis, 200 m and 400 m thick layers are reasonable for systems within 1 km of the axis. Permeability estimates for 2A layers from measurements in ophiolites, which are sections of oceanic crust and mantle that are exposed in the continental crustal rocks, are on the order of 10^{-12} to 10^{-10} m^2 (Nehlig and Juteau, 1988; van Everdingen, 1995). Wilcock and McNabb (1996) estimate permeabilities on the order of 10^{-13} to 10^{-12} m^2 based on observational studies of the Endeavour segment of the Juan de Fuca Ridge. For the models analyzed here, a permeability range of 10^{-10} m^2 to 10^{-14} m^2 was employed to capture the possible range of permeabilities for the mixing zone of layer 2A basalts.

A similar MOR system was modeled representing an anhydrite boundary separating the induced low-temperature circulation from the high-temperature discharge. Because anhydrite precipitates from heated seawater at temperatures ≥ 150°C (Bischoff and Seyfried, 1978) and is retrograde soluble at $T < 150$°C, the vertical wall was set to 150°C. Additional parameters include both 200 m and 400 m layer 2A thicknesses for analysis over a permeability range of 10^{-10} m^2 to 10^{-14} m^2. Similar to Figure 2b in Lowell et al. (2003), Figure 3.4 depicts the system's resulting circulation and anhydrite layer formation.

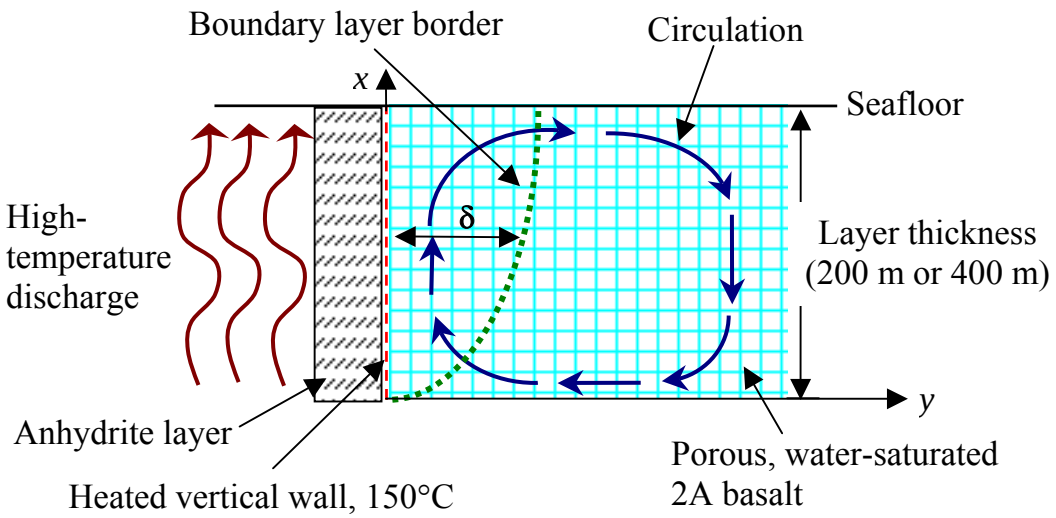

Figure 3.4: Sketch of a mid-ocean ridge hydrothermal system with an anhydrite boundary separating the high-temperature discharge from the 2A fluid filled basalt layer. Low temperature circulation occurs and a boundary layer forms close to the heated anhydrite wall. Symbols are defined in the List of Symbols on p. ix.

Lastly, near-axis convection was also modeled using steady-state boundary layer flow. Data from Dunn et al. (2000) suggest that a near-axis system has a vertical wall

temperature of about 1100°C and a height of about 5 km (Figure 1.1). However, for this analysis, a temperature of 600°C was used since crust is typically considered to be impermeable at a temperature between 600°C and 800°C (Manning et al., 2000). Figure 3.5 depicts the model set-up. The model was analyzed over a permeability range of 10^{-10} m^2 to 10^{-14} m^2.

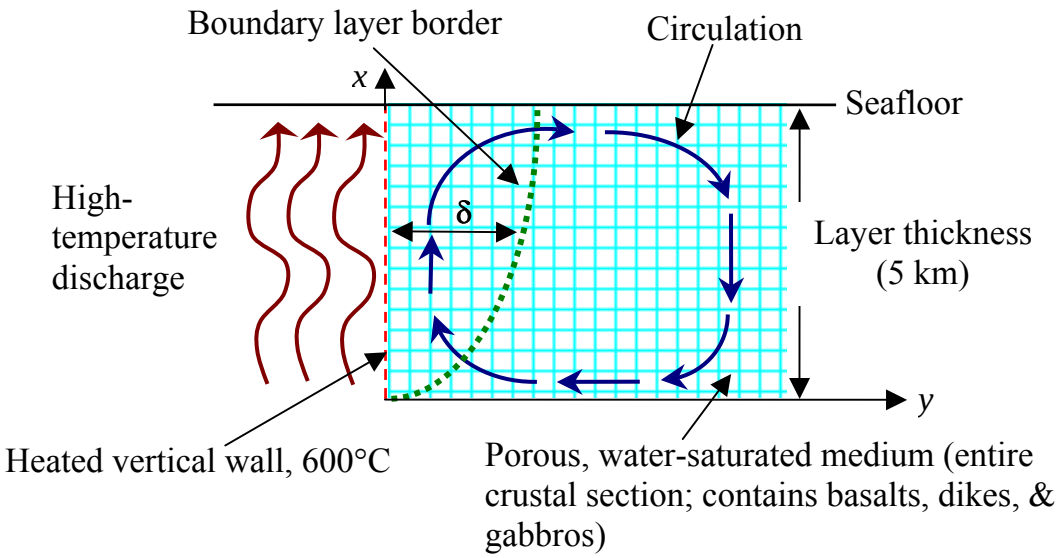

Figure 3.5: Hydrothermal flow steady-state boundary layer model for near-axis convection (layer thickness = 5 km). Sketch shows resulting boundary layer and low temperature circulation. Symbols are defined in the List of Symbols in p. ix.

3.3 Results

Boundary layer thicknesses were calculated along the quasi-vertical wall for all systems using values shown in Table 3.1. Values were calculated using equation (2.27). An underling assumption of boundary layer theory is that the thickness of the boundary layer δ is considerably less than the height of the wall H. Nominally, one might consider this condition is satisfied if $\delta/H \sim 0.1$. Here the condition is liberalized slightly and the theory

is employed for δ/H up to ~ 0.2. Layer thickness results were compared to the respective system's wall height over the stated range of permeabilities for each oceanic hydrothermal system described above to determine where the boundary layer theory was applicable.

Table 3.1: Values used in terrestrial submarine calculations (Cheng and Minkowycz, 1977). Variable definitions are given in the List of Symbols p. ix.

Variable	Value	Units
$c_{p,f}$	4.18	$kJ(kg°C)^{-1}$
g	9.8	ms^{-2}
K	1.0E-14 to 1.0E-10	m^2
k	2.60E-03	$kJ(sm°C)^{-1}$
T_w	varies	°C
T_∞	4	°C
x	varies	km
α	6.30E-07	m^2s^{-1}
β	1.80E-04	$°C^{-1}$
μ	2.70E-04	Nsm^{-2}
ρ_∞	1000	kgm^{-3}

Boundary layer thicknesses for systems containing a ratio of layer thickness to wall height of 20% or less are reported in Figure 3.6. Results show that boundary layer thickness varies as $K^{-1/2}$. This scaling is expected from equations (2.15) and (2.27) for the boundary layer calculations in Chapter 2.

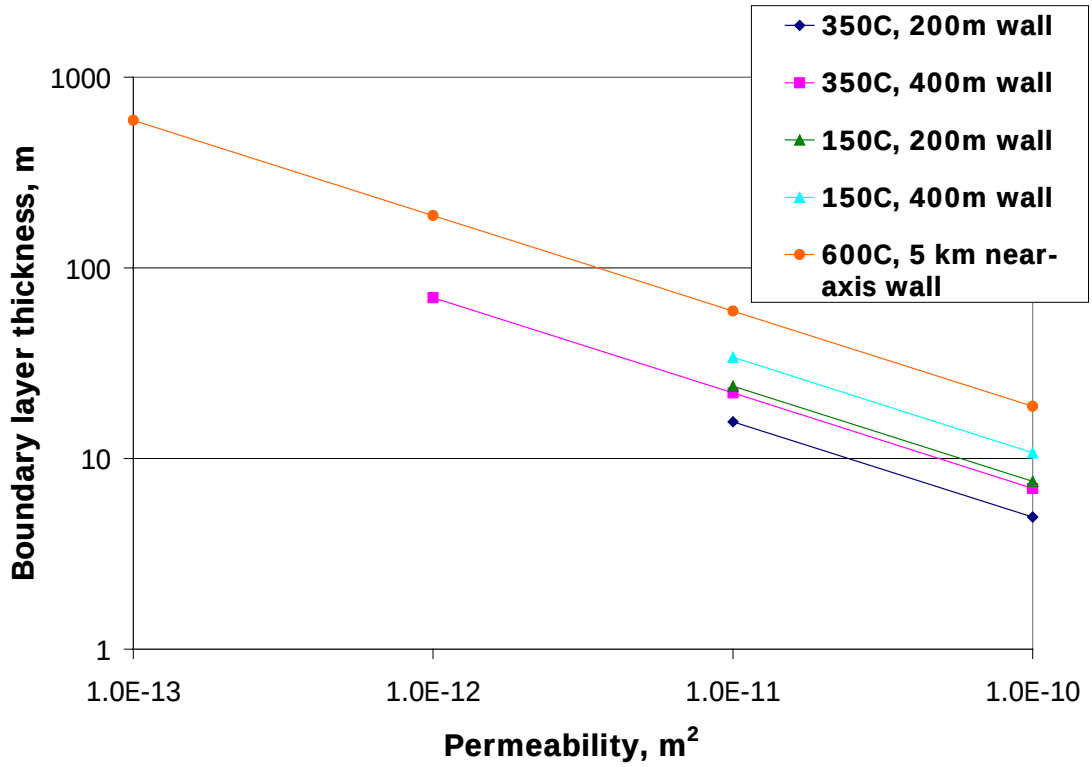

Figure 3.6: Boundary layer thickness for hydrothermal flow near high-temperature vent (350°C for 200 and 400 m thick layers), at a high-temperature vent with an anhydrite layer (150°C for 200 and 400 m thick layers), near a dike (600°C for 1 km thick layer), and for a near-axis convection system (600°C for a 5 km thick layer). Values were assessed at permeabilities between 10^{-10} to 10^{-14} m^2. The figure shows results where boundary layer theory is relevant (where boundary layer thickness is 20% or less than wall height).

In addition to boundary layer thicknesses, heat outputs for each hydrothermal system were calculated using equation (3.1) over the permeability range where the ratio of layer thickness to wall height was 20% or less. First, density change over boundary layer width was calculated using equation (2.5), where the value of T is dependent on it's location (y,x). Then, using each resulting value of ρ_f and values from equations (2.24) and (2.26), the energy transport for a certain dike depth was calculated by integrating equation (3.1) over the thickness of the boundary layer, δ:

$$Q = \int_0^{\delta} \rho_f u T c_{p,f} dy \tag{3.1}$$

Results, given per kilometer of ridge length, are shown in Figure 3.7.

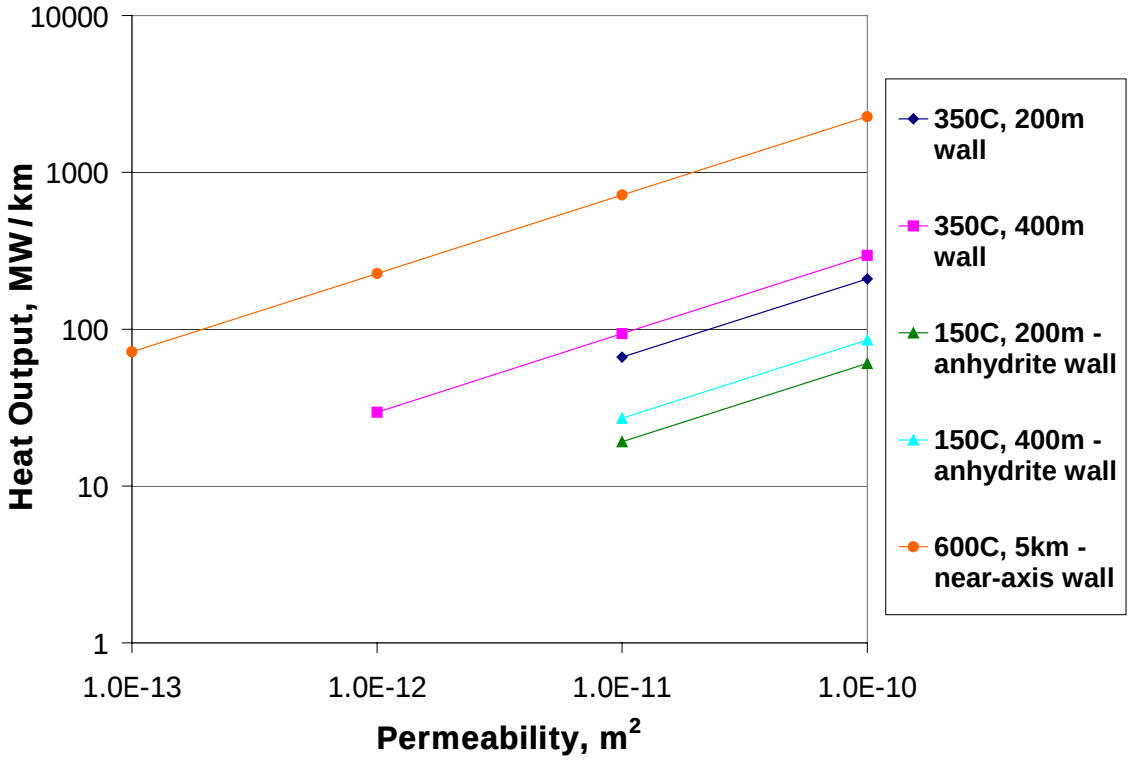

Figure 3.7: Heat output values for hydrothermal flow near high-temperature vents, at a high-temperature vent with an anhydrite layer, adjacent to a dike, and at a near-axis convection system. Values calculated for permeability range of 10^{-10} to 10^{-14} m^2. Results reported are for systems where boundary layer theory is relevant (where boundary layer thickness is 20% or less than wall height).

3.4 Discussion

3.4.1 Focused vs. diffuse flow systems

Results in Figure 3.7 show that heat output is highly sensitive to permeability and layer thickness. For the high-temperature, high-permeability, thick layer 2A focused flow systems, the boundary layer flow can transport about 300 MW/km of ridge axis. This value is of the same order as some observed transports at high-temperature hydrothermal systems (Ramondenc et al., 2006; Baker, 2007). At the other extreme, low-temperature diffuse flow, low-permeability, thin layer 2A systems transport about 20 MW/km. Since high-temperature ridge-crest hydrothermal systems typically have heat outputs of hundreds of MW/km, these results suggest that the fraction of heat output by diffuse flow is typically less than or equal to that of the high-temperature system. This result is consistent with that of Veirs (2006) for the Juan de Fuca Ridge, but it not consistent with the estimates of Schultz (1992), Ramondenc et al. (2006), and Rona and Trivett (1992).

As a means of verifying whether the results of this model are valid, other models for the relationship between high-temperature focused flows and low-temperature diffuse flows on the mid-oceanic ridge axis should be investigated. Rather than assuming diffuse flow is simply induced flow along a hot boundary, diffuse flow may result from mixing between a broad upwelling zone of the high-temperature fluid and seawater in the extrusives. Geochemical data from diffuse flow venting at the East Pacific Rise near 9°50′ N show that diffuse flow is a mixture of high-temperature hydrothermal fluid and seawater (Von Damm and Lilley, 2004). Figure 3.8 depicts this concept.

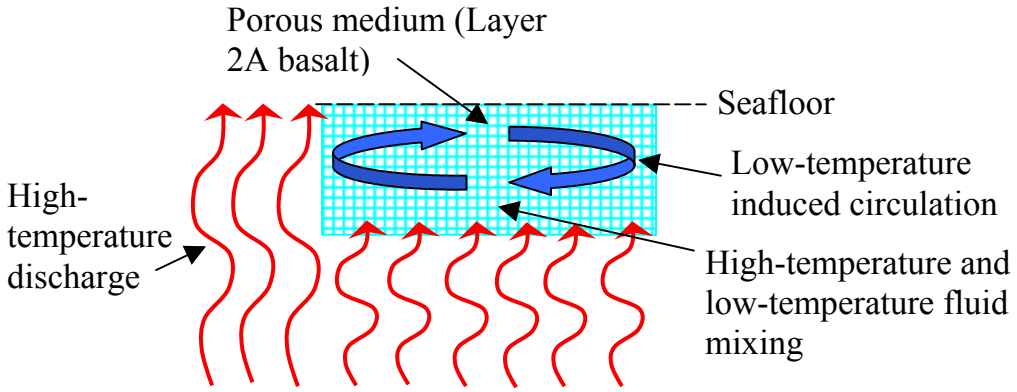

Figure 3.8: Model concept of cold seawater mixing with high-temperature fluid flow from below in the shallow seafloor.

3.4.2 Near-axis systems

Figure 3.7 also shows that the near-axis convection system is found to transport from ~80 to 2300 MW/km. These values are in reasonable agreement with the numerical results of Cherkaoui et al. (2003). Cherkaoui et al. (2003) investigated a near-axis oceanic system using a steady-state thermal model of crustal formation at a fast spreading ridge. Results showed that for a uniform permeability greater than about 4 x 10^{-14} m^2 and a "cracking temperature" of 800°C, hydrothermal circulation cools the crust and near-vertical isotherms form within a narrow width (less than 1 km) in 6 km deep crust (Figure 3.9). A "cracking" temperature is the temperature above which crustal rocks are considered impermeable and below which are assumed to be a porous continuum (Manning et al., 2000). For this permeability range and cracking temperature, the results agree well with the steep, compact isotherms converted from the seismic data collected by Dunn et al. (2000). When comparing the study performed with the boundary layer theory, the thicknesses of the isotherms for permeabilities greater than 1 x 10^{-13} m^2 are also less than

1 km thick. Also, the cracking temperature assumed by Cherkaoui et al. (2003) agrees well with the specified 600°C temperature used in the boundary layer analysis.

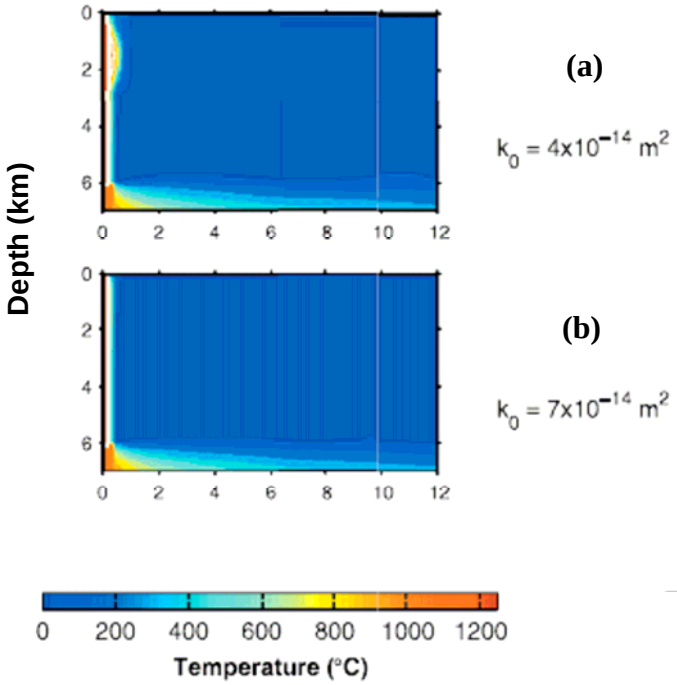

Figure 3.9: Modified results figure from Cherkaoui et al. (2003) for an 800°C "cracking" temperature and permeabilities of (a) $k_0 = 4 \times 10^{-14}$ m^2 and (b) $k_0 = 7 \times 10^{-14}$ m^2 showing the narrow isotherm width of < 1 km for depths up to 6 km.

Both the boundary layer model considered here and Cherkaoui et al (2003), assume steady-state conditions. This supposition requires that the rate of heat input from the partially molten zone (Figure 1.1) equal the heat output from the boundary layer flow. The average rate of heat input, Q_{in}, from the mushy zone can be determined from the average spreading rate and the latent heat, L, of the melt. For a half-spreading rate of $\langle v \rangle$ = 3 cm/yr is:

$$Q_{in} = \rho_m \langle v \rangle LH \quad (3.2)$$

where ρ_m is the density of the magma, and H is the height of the magma intrusion. From equation (3.2), $Q_{in} \approx 6 \times 10^3$ W/m. Comparison of this value to the boundary layer heat flow results shows that the rate of heat input from the partially molten crust is < 10% of the hydrothermal heat output. This result indicates that the extent of the mushy zone in the lower crust inferred from seismic studies might not be a steady-state feature as previous studies (e.g., Cherkaoui et al., 2003) have assumed.

3.4.3 Boundary layer theory assumptions

The boundary layer model investigated here makes several assumptions that warrant consideration. The fact that boiling may occur in the system is not considered since the boundary layer theory assumes the fluid is always in the liquid phase. Also, the theory obtains a steady-state solution that occurs for a constant temperature wall and does not consider the response of the boundary layer if wall temperature declines. This may be particularly important for the near-axis system, which does not appear to be in a steady-state. Additionally, for the models used in this investigation, the water within the porous medium was assumed to be pure water with thermal properties independent of temperature. The models should consider that in reality the fluid is not pure and its properties change significantly with temperature. Incorporating these property dependencies into the model could change the buoyancy and heat transfer rates.

3.5 Conclusions

This study employed boundary layer theory in order to gain a more detailed understanding of hydrothermal circulation in the oceanic crust. In particular, the fractionation of heat transfer between high-temperature focused flow and low temperature diffuse flow at mid-ocean ridges and near-axis convection systems were investigated. Results of the analysis indicated that diffuse flow might account for up to 50% of the total hydrothermal heat output at mid-ocean ridges. This result is at the lower end of previous estimates; however, other models for diffuse flow need to be considered before this result can be confirmed. For near-axis circulation, results from treating the circulation as a steady-state boundary layer flow agree well with isotherms inferred from seismic data studies (e.g., Dunn et al., 2000) and Cherkaoui et al.'s (2003) numerical modeling results including similar boundary layer thicknesses, isotherm behaviors, and wall temperatures. A heat balance calculation suggested that to match the observed isotherm distribution, the rate of heat input from the partially molten lower crust must be significantly greater than that provided by the seafloor spreading, indicating that the width of the partially molten zone may evolve over time. Although boundary layer theory makes many simplifying assumptions, the models obtain reasonable solutions that provide insight into key processes occurring in oceanic hydrothermal systems. These results can also lead to further understanding of the transport of chemical constituents in diffuse flow and near-axis hydrothermal fluids and their relationship with the biological systems occurring there.

CHAPTER 4. MARTIAN HYDROTHERMAL CIRCULATION MODELING

4.1 Introduction

In March of 1972, the spacecraft Mariner 9 took the first close up pictures of the Martian landscape. Vast canyons, gigantic volcanoes, and numerous winding channels and valleys were visible at a much higher resolution than ever before. The two Viking orbiters took additional photographs in the late 1970s, and from about 1997 until 2001 the Mars Orbiter Laser Altimeter (MOLA), aboard the Mars Global Surveyor (MGS) provided additional, higher resolution pictures. Currently, the Mars Reconnaissance Orbiter (MRO), launched in 2005, uses an instrument called the High Resolution Imaging Science Experiment (HiRISE) to obtain visual range images with resolutions of up to 30 cm. These extremely detailed photographs provide a tremendous amount of information about our neighboring planet.

The spacecraft observations revealed that current conditions on Mars are cold and dry. At the surface, the Martian atmosphere is more than 100 times less dense than Earth's and contains only minute amounts of water vapor (Baker, 2001). The atmosphere is mostly made up of CO_2 and temperatures average around -53˚C (Jakosky and Phillips, 2001). At the equator, around mid-day, temperatures can rise above freezing; yet water is still not able to remain in liquid form for long periods if exposed to the dry Martian atmosphere at the surface due to the low atmospheric pressure (Jakosky and Phillips, 2001). According to laboratory experiments performed by Sears and Moore (2005), pure water evaporates at just under 1 mm/h on the Martian surface. Therefore, liquid water can only remain on

the surface for a significant period of time if the flux of water to the surface is greater than the evaporation rate, if the fluid is a water mix (combined with mud, salt, etc.) and/or if the atmosphere was denser.

Although the present climate is not ideal for surface-water existence, Mars may have had a denser atmosphere and a warmer average temperature in the past. The denser atmosphere could have been formed as a result of volatile inputs related to global volcanism (Cloy, 1984). These factors would have enabled a period of climate with rainfall, which may explain the widespread valleys found on the older southern highlands (Pollack et al., 1987). There is also evidence that craters underwent greater erosion early in history, which indicates a denser atmosphere in the past (Schultz, 1985).

The age of the surface that valleys and channels cut through helps determine when the valleys and channels developed. Three factors determine the age of a Martian surface area: the density of craters; comparison to lunar crater density; and radiometric dating of Martian meteorites (Hartman, 2001). The Noachian epoch, which ended about 3.5 billion years ago (Ga), is indicated by heavily cratered terrain, followed by the Hesperian epoch (from about 3.5 to 3 Ga), which is moderately cratered, and ending with the Amazonian epoch (from about 3 Ga to present), which is mostly smooth with few craters (Hartman, 2001). The fewer craters an area contains, the younger the surface. This is a result of a decrease in meteoritic impacts over time and erosion and lava flows creating a smooth, new, young surface over the older cratered one. Valleys showing rainfall erosion

characteristics are believed to have formed during the Noachian period since they mostly appear on the more densely cratered terrain (Pollack et al., 1987).

One problem with rainfall as the only source of valley formation, however, is that spacecraft observations show that valleys and channels have formed since this the Noachian epoch. Images obtained by MGS cameras depict fluvial valleys located on craterless regions, indicating they occurred recently in geologic time (Baker, 2001). Additionally, young lava flows on the western side of Ceraunius Fossae, a region north of the Tharsis bulge, have fluvial flows overlaying them, meaning that they are even more recent than the lava flows (Mouginis-Mark, 1990).

A number of other observations also argue against rainfall as the only mechanism for shaping surface morphology. These include, for example, recent evidence of possible fluid flows on the surface (see Figure 1.2), observations of valleys that display sapping morphology instead of runoff characteristics, and the fact that isolated valley systems exist. The isolated systems indicate a local source of fluid flow (Brakenridge et al., 1985; Gulick, 2001; 1998) or sapping processes as opposed to a global climate change. Regions near two large volcanoes, Tharsis and Elysium, in the northern plains contain sizeable outflow channels that are believed to have formed by catastrophic release of frozen subsurface volatiles during the late Hesperian into the Amazonian periods (Jakosky and Phillips, 2001). Magma chambers within the volcanic edifice may have heated nearby groundwater forming a subsurface hydrothermal system. Over time, the hot hydrothermal fluids could have induced melting in permafrost near the surface, which

then discharged to form the observed channels (Gulick, 1998). Dissociation of subsurface hydrates driven by the hydrothermal system may also have formed the geomorphology observed (Rodriguez, 2006). Smaller channels have been mapped (Bleacher et al., 2007; Trumble, et al., 2008) in the same region that are found to have similar morphologies and therefore may have formed through similar processes.

Impacts, lava flows, and magmatic intrusions all may have provided local heat sources to drive hydrothermal processes that might have formed channels, valleys and other surface morphology. Heat resulting from impacts can melt the underlying permafrost and cause water to upwell to the surface (Rathbun and Squyres, 2002; Brakenridge et al., 1985; Newsom et al., 1996). Lava flows could also heat surrounding groundwater and release it to the surface. The discharged water would leave space between soil particles, causing the ground to compact and the surface level to drop (Squyres et al., 1987) and form channels.

Overall, many theories about the formation of Martian surface morphology exist. However, evidence of recent morphology formation (e.g. Malin and Edgett, 2000) argues for local hydrothermal system formation mechanisms and warrants further investigation. Previous quantitative analyses performed on Martian hydrothermal systems include a magma intrusive driven system by Gulick (1998), impact driven systems by Rathbun and Squyres (2002) and Abramov and Kring (2004, 2005), and sills and lava flows melting ground ice by Squyres et al. (1987). This project focused on magma intrusion systems similar to Gulick (1998).

In previous models for magma intrusion driven hydrothermal systems on Mars, coarse spatial and temporal resolutions were used which made temperatures and velocities close to the chamber difficult to observe. Fluid behavior close to the chamber proves important as shown in Gulick (1998) results where a large change in temperature within < 100 m is evident. By employing the boundary layer theory, fluid behavior within close proximity to the chamber can be studied in detail. Results from the boundary layer analysis can then be compared with requirements for the formation of various fluvial features predicted by previous studies (see Figure 4.5) to determine if hydrothermal flow is a feasible formation mechanism. Connections between heat and mass flows and certain surface feature formation requirements have not been performed previously.

4.2 Model

To gain a basic understanding of a hydrothermal system adjacent to a magma intrusion located just beneath the surface and to find if such a system may be feasible for forming Martian surface features, a steady-state boundary layer model was employed (Cheng and Minkowycz, 1977). This theory was chosen, in part, after reviewing results obtained by Gulick (1998) for hydrothermal circulation near the wall of a cooling intrusion (see Figure 4.1) that showed the majority of temperature change occurred within a relatively narrow region near the intrusion boundary.

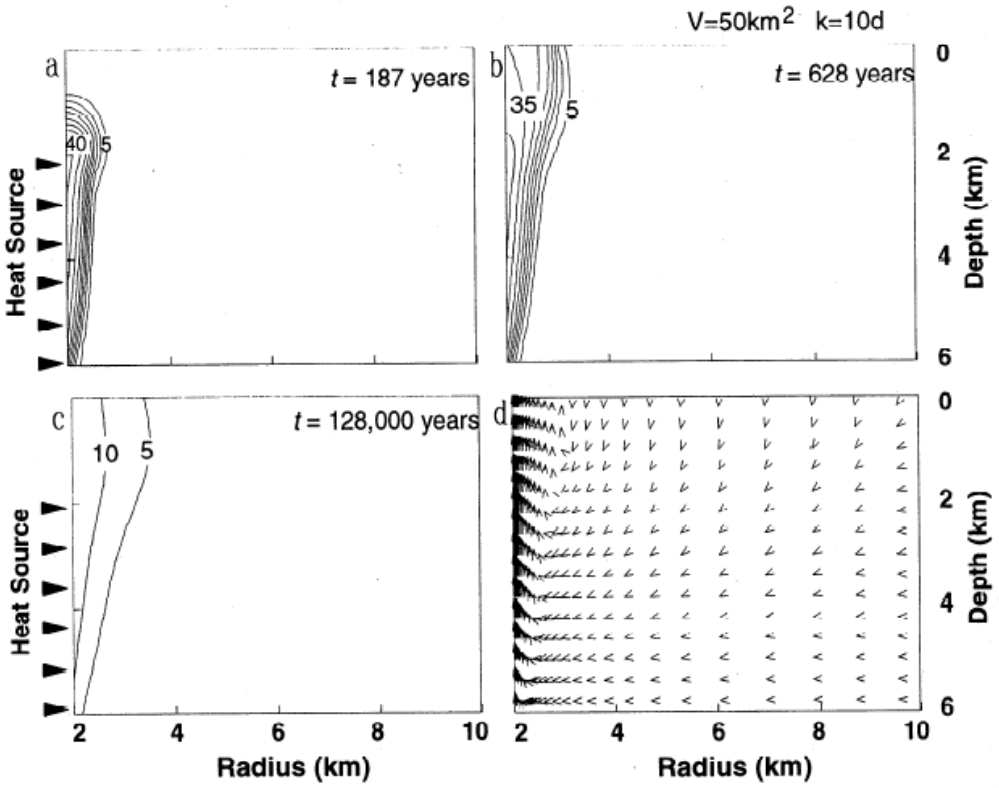

Figure 4.1: Gulick (1998) results for a 50 km^3, 4 km deep, magma intrusion within a permeable medium with K = 10^{-11} m^2 (10 darcys). Figure taken from Gulick (1998).

The model used for this investigation consisted of water-saturated porous Martian regolith located next to a magma intrusion wall held at a constant temperature as depicted in Figure 4.2. An analytical solution was obtained as described in Chapter 2. First, velocities and temperatures were calculated with equations (2.24), (2.25), and (2.26) (Cheng and Minkowycz, 1977). Using these results we calculated the total energy transport and volume flux for various intrusion depths and regolith permeability. Density of the fluid at a given height was calculated using equation (2.5). Parameter values were taken from Table 4.1.

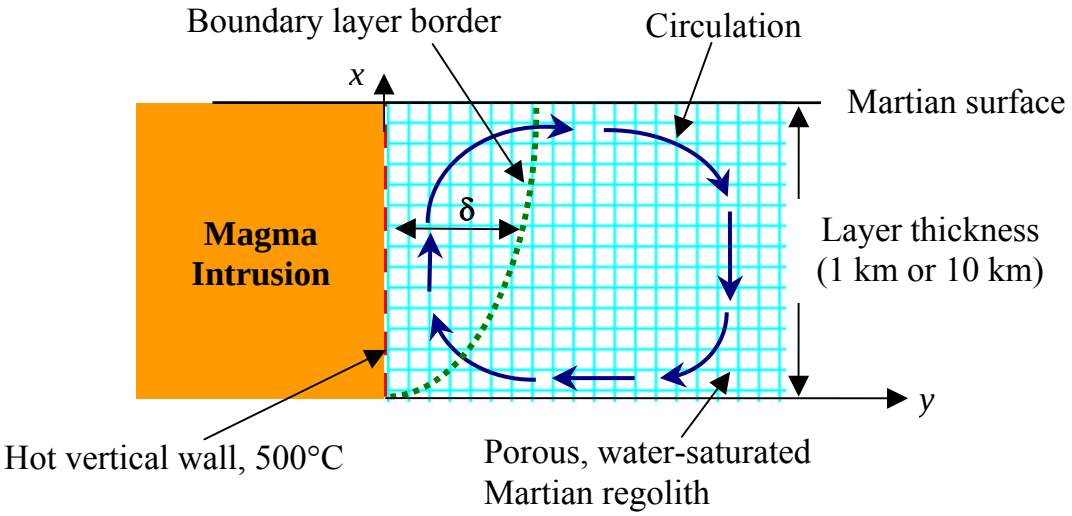

Figure 4.2: Steady-state boundary layer model of magma intrusion driving hydrothermal circulation on Mars. Symbols are defined in the List of Symbols in p. ix

Table 4.1: Variable values used for conditions on Mars for basaltic regolith and magmas. (Martian values taken from Gulick, 1998). Variable definitions are given in the List of Symbols p. ix.

Variable	Value	Units
$c_{p,f}$	4.18	$kJ(kg°C)^{-1}$
g	3.72	ms^{-2}
K	1.0E-14 to 1.0E-08	m^2
k	3.50E-03	$kJ(sm°C)^{-1}$
T_w	500	°C
T_∞	4	°C
x	1 or 10	km
α	8.38E-07	m^2s^{-1}
β	4.59E-04	$°C^{-1}$
μ	1.00E-03	Nsm^{-2}
ρ_∞	1000	kgm^{-3}

Then, using the value of ρ_f from equation (2.5) and values from equations (2.24) and (2.26), the energy transport for a certain dike depth was calculated by integrating

equation (3.1) over the thickness of the boundary layer, δ. Similarly, the mass flux, Φ_m, for a certain depth dike was calculated by integrating equation (4.1) over the thickness of the boundary layer:

$$\Phi_m = \int_0^{\delta} \rho_f u dy \tag{4.1}$$

4.3 Results

Figure 4.3 depicts the heat transport within the boundary layer and Figure 4.4 depicts the volume flux within the boundary layer at the top of 1-km- and 10-km-deep intrusions for various regolith permeabilities. The apparent dependency of heat and volume flux on permeability is apparent. Figure 4.4 shows that a 10-km-long dike with a height of about 5 km injected into a highly permeable rock would transport about 1 km^3/yr of fluid.

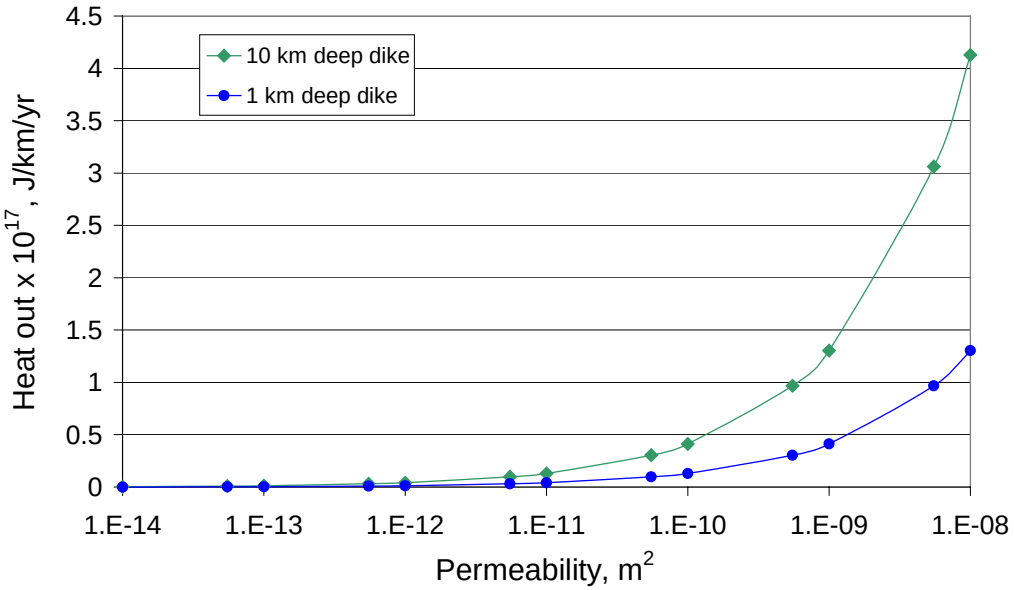

Figure 4.3: Heat out for 1-km- and 10-km-deep dikes over a range of Martian crustal permeabilities in steps of half an order of magnitude. Permeability range covers reasonable values for consolidated basaltic regolith (≤ 1E-08 m^2) and that allow fluid movement (≥ 1E-14 m^2).

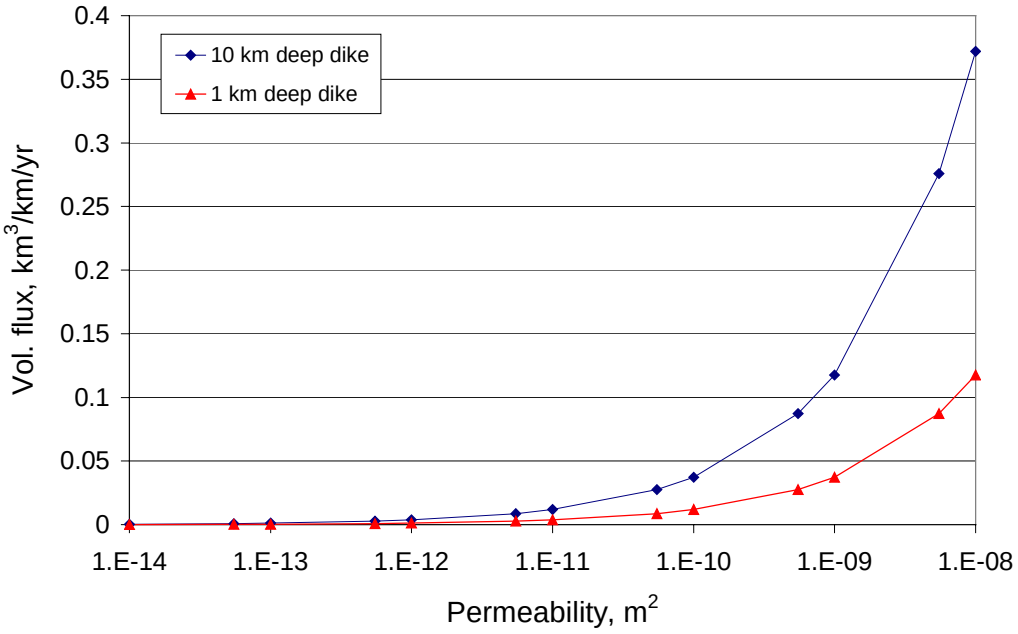

Figure 4.4: Volume flux for 1-km- and 10-km-deep dikes over a range of possible Martian crustal permeabilities in steps of half an order of magnitude. Permeability range covers reasonable values for consolidated basaltic regolith (≤ 1E-08 m^2) and that allow fluid movement (≥ 1E-14 m^2).

A hydrograph by Kraal (2007) (personal communication), Figure 4.5, depicts estimates of total water volume versus duration of water flow required to form certain Martian geomorphic surface features. For the 10-km-long, 5-km-deep dike magma-hydrothermal system that produces about 1 km^3/yr of fluid flow, comparison of the volume flux results to this hydrograph suggests that a significant amount of time is required to produce enough flow to form observed surface morphologic features.

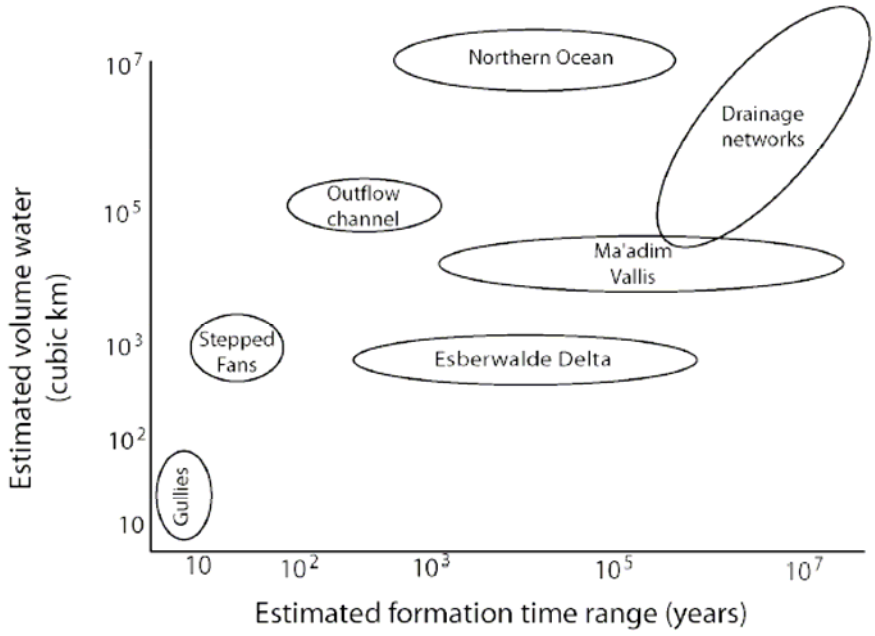

Figure 4.5: Hydrograph depicting ranges of required water flow volumes for formation times of various Martian morphologies calculated by Martian models (personal communication, Kraal, 2007).

4.4 Discussion and Conclusions

Although mass fluxes from the boundary layer model suggest that hydrothermal flow from a single intrusion on Mars requires an unreasonable amount of time to form surface features shown in Figure 4.5, multiple systems contributing to the same feature may enable formation. Also, there is considerable evidence of both water ice (e.g., Clifford, 1993; Plaut et al., 2007; NASA, 2008) and gas hydrates (e.g., Max and Clifford, 2001; Rodriguez et al., 2005, 2006) just beneath the surface of Mars. Heat transport from a hydrothermal system may melt a layer of frozen ice under the surface causing the fluid outflow levels to adequately increase for feature formation or dissociate subsurface gas hydrates causing surface alteration. Calculations to determine fluid flux produced from a layer of subsurface ice can be performed by considering a region of constant heat flux

beneath a solid layer with a temperature below freezing on Mars. Melting of the ice layer will occur at a rate of $t^{-1/2}$ (Carlsaw and Jaeger, 1959), yet an exact solution for fluid flux with a heat flux boundary is not available.

Although the boundary layer model provides a reasonable first estimate of the fluid flux that can be expected from a Martian hydrothermal system, the model invokes assumptions that need further consideration. In this model the fluid properties are assumed to be constant, whereas they actually vary strongly with temperature and pressure. Both β and μ decrease significantly with increasing temperature, thus increasing the buoyancy of the fluid. Heat and mass fluxes from the model used here are therefore underestimates. Another assumption is that the system exists at steady-state. This assumption provides no information on how long the system takes to reach steady-state and does not consider the decline in heat supplied by the magma intrusion as it cools over time. By assuming steady-state flow near an isothermal high-temperature wall, the mass and heat fluxes are overestimated, compared to those from a cooling intrusion. The effects of these two assumptions may therefore partially cancel each other. The boundary layer theory employed here also assumes that the fluid remains in the liquid phase and does not consider the effects of boiling and vapor phase transitions on the fluid and heat fluxes. The enhanced heat transport resulting from boiling and transport of high enthalpy vapor may be important during the early phase of hydrothermal circulation before the magma body has cooled significantly. Moreover, the groundwater is likely to be saline and two-phase flow in a saline fluid affects the dynamics of heat and mass transport. Lastly, the model assumes an unlimited source of fluid when, in reality, the amount of

subsurface fluid in the Martian regolith is unknown and may significantly restrict the fluid mass discharge.

A similar model of a Martian hydrothermal system (Gulick, 1998) used the program SUTRA (Voss, 1984) to study circulation driven by cylindrical magma chambers of different volumes. Gulick (1998) determined that the maximum discharge volume flux for a 4-km-tall magma chamber 2 km below the surface, with a volume of 50 km^3, initial temperature of 1250°C, and adjacent medium permeability of 10^{-11} m^2 was just less than 3,000 kg/s after about 600 years. Estimating from results depicted in Figure 4.4 for a 5-km-deep, 10-km-long, constant temperature wall (dike intrusion) at 500°C and an adjacent medium permeability of 10^{-11} m^2, the volume flux equals 0.1 km^3/yr, which converts to about 3,200 kg/s. This mass flux rate is comparable to the results obtained by Gulick (1998).

Overall, boundary layer theory provides informative insight into the behavior of Martian hydrothermal systems driven by a magmatic intrusion. Heat and mass flux results determined that a single magma intrusion is not capable of forming surface morphology in a reasonable amount of time. However, if other contributing factors are considered, such as ice melt and hydrate dissociation, analyses may show that magma driven hydrothermal systems on Mars can form surface features.

CHAPTER 5. SUMMARY AND FUTURE WORK

5.1 Summary

Hydrothermal systems contribute to a planet's geochemical cycling, heat and mass flux budgets, and on Earth are particularly important as a result of extensive volcanism associated with generating new lithosphere. Additionally, terrestrial systems serve as energy resources and as agents for ore formation. On other planets, these systems may provide habitats for life. Martian hydrothermal processes may also have formed the fluid-like morphology observed on the surface. Therefore, understanding hydrothermal systems on Earth and other planetary bodies will greatly assist in the investigation of planetary processes.

Chapter 2 presented the underlying theory and methodology used to analyze hydrothermal systems in this thesis. Chapter 3 analyzed two hydrothermal cases in the oceanic crust. One concerned the fractionation of hydrothermal heat output between high-temperature and low-temperature discharge at mid-ocean ridges. The second investigated "near-axis" convection at the transition between magma-driven high-temperature circulation along ocean ridge axes and low-temperature circulation occurring off-axis as the lithosphere ages. Boundary layer theory results showed that low-temperature diffuse flow contributes 50% or less of the heat output in a mid-oceanic ridge system. This estimate is at the lower end of estimates from rather limited data sets, and other models of diffuse flow should be investigated before the results of the boundary layer model can be confirmed. The near-axis temperature distribution derived from boundary layer theory

was in reasonable agreement with that inferred from seismic tomographic studies of the oceanic crust (Dunn et al., 2000) and with other numerical models (e.g., Cherkaoui et al., 2003). Results from the boundary layer analysis also showed that for a given permeability, the near-axis system produced more heat flux than either the focused or diffuse ridge system flows. Lastly, the model also indicated that heat transfer in the hydrothermal boundary layer was greater than that input from steady-state generation of the oceanic crust by seafloor spreading. Therefore, although the spreading rate was considered to be constant for this timescale (on the order of thousands of years), analysis results suggest that the system is not at steady-state and the size of the mushy zone indicated by seismic studies may change with time. Chapter 4 considered a magma-driven hydrothermal system on Mars. Results showed that fluid outflow adjacent to a single intrusion was too small to generate observed Martian surface features in a reasonable length of time.

5.2 Future Work

The hydrothermal models analyzed with the steady-state boundary layer theory, for both terrestrial submarine and Martian systems, involved a number of assumptions that require further consideration. For example, the models as presented involved only single-phase flow. Boundary layer theory does not consider that the water in the saturated medium may change to the vapor phase during circulation. This phase change will alter the heat flux and the fluid flux to the surface. Also, the models assume that the vertical wall remains at a constant temperature. In reality, the hot vertical wall will cool over time. A finite control-volume code, the Fully Implicit Hydrothermal Event Simulator (FISHES), developed at Georgia Tech by Kayla Lewis (Lewis, 2007) can take into account two-

phase flow and time-dependent temperature change. FISHES can therefore provide more accurate results for hydrothermal circulation on both Earth and Mars. Additionally for Mars, FISHES can consider the lower Martian gravity and pressure.

Improvements in the model can be gained by considering other fluids than just pure water. FISHES can consider saline fluids, which are suggested to exist on Mars (Brass, 1980; Knauth and Burt, 2002; Burt and Knauth, 2003). Two-phase flow in saline fluids may result in the formation of a dense, thermodynamically stable brine solution that can remain a fluid on the surface of Mars longer than pure water and would therefore have more time to carve features (Sears and Chittenden, 2005). Also two-phase flow in saline fluids is dynamically different from pure water (e.g., Lewis, 2007), which affects the transport dynamics of Martian hydrothermal flows. The FISHES code assumes saline fluid parameters and is able to calculate temperatures, velocities, and boundary layer thicknesses that are then used to determine heat output and fluid mass flux. Results would provide knowledge of Martian saline fluid hydrothermal system behavior and can give insight into how the system changes for different fluid types.

Although model results suggested that fluid flow from a Martian hydrothermal system driven by a magma intrusion was too small to produce surface features, other considerations such as multiple systems contributing to the same feature, the melting of subsurface ice, or hydrate dissociation may increase the flux or disrupt the surface enough to form a feature. During heat transfer from the magma chamber to groundwater, the warmed groundwater may slowly melt permafrost. This will increase the outflow to

the surface by increasing the fluid volume and also by removing a low permeability layer that hindered fluid access to the surface. The Martian intrusion model will incorporate the permafrost layer by considering a low permeability layer and calculating fluid temperatures that reach the layer. Depending on the temperatures reaching the ice layer, the time it will take to melt the ice and the amount of fluid volume released can be determined. Effects of the cold water released on the temperature of the circulating fluid should be considered as well as the different ice layer thicknesses possible. Clifford (2003) estimated that the thickness of the subsurface ice in Mars' equatorial area (± 20°) ranges from 0 to ~11 km, with a nominal value of 2.27 to 2.47 km based on calculated crustal temperature distribution. Hydrate dissociation can also possibly form surface features by releasing gas and expulsing fluid from the ground (Rodriguez, 2006). With these additional contributors, Martian hydrothermal systems may be adequate morphology formation mechanisms.

Additional terrestrial seafloor hydrothermal system modeling improvements can be accomplished by incorporating anhydrite precipitation directly into the model and by considering other models of diffuse flow that directly involve mixing between high-temperature fluids and seawater at mid-ocean ridges. Induced circulation of seawater as described by boundary layer theory, may not be the only means of generating low-temperature diffuse flow. The mixing of seawater in the shallow crust and high-temperature discharge might instead occur throughout the crustal layer or in a thin layer near the seafloor. Further insight would be gained into oceanic hydrothermal system behavior through analyzing the induced circulation and resulting heat and fluid fluxes.

Field studies directed towards measuring rates of diffuse flow, along with obtaining data on diffuse flow chemistry could help constrain models of diffuse flow.

A field study could provide heat flow data for improving near-axis hydrothermal system modeling. However, near-axis systems prove difficult to locate and identify. Since these systems occur where circulation transitions between on axis magma-driven high-temperature circulation and low-temperature off-axis circulation occurring as the lithosphere ages, they are hard to distinguish from the surrounding systems. For this reason as well, heat flow measurements are also hard to obtain since there may be uncertainty as to if the flow is near-axis or on axis.

APPENDIX A

U-substitution *Matlab®* programs:

```
% Program for solving high order differential equation for boundary
% layer modeling.  Value for the initial condition η= 0, f'' = u3 = ?

% Written by K. Craft, 2007

% Bldrive.m

u0=[0 1 -.444];
etaspan = [0 10];

[x u]=ode45('RHSf', etaspan, u0);
% ode45 is a matlab function used to solve ordinary differential equations

figure(1)
plot(x, u(:,1),'r');
figure(2)
plot(x, u(:,2),'r');
figure(3)
plot(x, u(:,3),'r');
```

```
% RHSf.m
% Function representing right hand side of equations for u-substitution method

% Written by K. Craft, 2007

function fprime3 = RHSf(eta, u)  % 'fprime3' denotes right hand side of high order equations
fprime3 = [u(2); u(3); -0.5*u(1)*u(3)];
end
```

Fortran program to solve for f, f′, and f″ values:

```
C**********************************************************************
C       Subroutine BLSOLV
C
C       Written by K. Craft, 2007
C
C       Solves the similarity equations for the boundary layer problem
C        of fluid flow about a vertical, flat plate using the Euler
C        forward method
C
C       Values are stored for f, f', and f''
C
C       Variables:  N, M: Indexing Integers
C                   U1, U2, U3:  variables which represent partial
C                                differential equations
C                   DX = step size distance from wall of intrusion
```

```
C*****************************************************************

      SUBROUTINE BLSOLV (N, DX)

      IMPLICIT NONE
      INTEGER N, M
      DOUBLE PRECISION U1(N), U2(N), U3(N), DX

      U1(1) = 0.D0
      U2(1) = 1.D0
      U3(1) = -.442

      OPEN(40,FILE='f1d.data',STATUS='UNKNOWN')
      OPEN(50,FILE='fprime1d.data',STATUS='UNKNOWN')
      OPEN(60,FILE='f2prime1d.data',STATUS='UNKNOWN')

160   FORMAT(F30.16)


      WRITE(40, FMT=160) U1(1)
    WRITE(50, FMT=160) U2(1)
    WRITE(60, FMT=160) U3(1)

      DO M = 1, N-1
        U1(M+1) = U1(M) + DX * U2(M)
        U2(M+1) = U2(M) + DX * U3(M)
        U3(M+1) = U3(M) - DX * 0.5 * U1(M) * U3(M)

        WRITE(40, FMT=160) U1(M+1)
        WRITE(50, FMT=160) U2(M+1)
        WRITE(60, FMT=160) U3(M+1)
      ENDDO

      CLOSE(40)
      CLOSE(50)
      CLOSE(60)

      RETURN

      END
```

Fortran program to solve temperature and velocity values:

```
C*****************************************************************
C     Program to calculate values for x-grid values at certain Y and also
C     calculates the u and v velocities, temperatures and densities by
C     using eta, f, and fprime values
C
C     Written by K. Craft, 2007
C
C     Variables:
C       N, I: Indexing values
C       K = permeability of country rock [m^2]
```

```
C         g = gravity (Mars_g=0.38* Earth_g)  [m/s^2]
C         B = thermal expansion coefficient [m^3/degC]
C         TW = temperature at the magma wall [degC]
C         TINF = temperature of water infinitely far away from wall [degC]
C         RHOINF = density infinitely far away from wall [kg/m^3]
C         KM = thermal conductivity of medium [kJ/s/m/degC]
C         CPF = specific heat of fluid [kJ/kg/degC]
C         ALPHA = KM/RHOINF/CPF [m^2/s]
C         MU = viscosity of fluid [N*s/m^2]
C          RA = Rayleigh number for a porous medium [unitless]
C          X = x-coordinate
C          Y = y-coordinate
C          ETA = dimensionless similarity variable
C          F = value representing f(eta)
C          FPRIME = value equal to (T-Tinf)/(Twall-Tinf)
C          FPRIME2 = second derivative of F
C          TEMP1D = current temperature at a x location
C          DENSITY = current density at a x location
C*************************************************************************


          SUBROUTINE VELTEMPDEN (N, DX)

          IMPLICIT NONE
          INTEGER N, I
          DOUBLE PRECISION K, g, B, TW, TINF, RHOINF, KM
          DOUBLE PRECISION CPF, ALPHA, MU, RA, Y
          DOUBLE PRECISION DX, X(N), ETA(N), F(N), FPRIME(N), U(N), V(N)
          DOUBLE PRECISION TEMP1D(N), DENSITY(N)

150       FORMAT(F30.16)
160       FORMAT(F30.24)

          OPEN(40,FILE="f1d.data",STATUS='OLD')
          OPEN(50,FILE="fprime1d.data",STATUS='OLD')


c         MARS VALUES (Replaced with terrestrial values for hydrothermal systems on
c        Earth)

          Y = 4000.D0
          K = 1.0D-10
          g = 9.8*0.38
          B = 0.459D-3
          TW = 500.D0
          TINF = 4.D0
          RHOINF = 1000
          KM = 2.6D-3
          CPF = 4.18
          ALPHA = KM/RHOINF/CPF
          MU = 1.D-3


          RA = K*g*B*Y*(TW-TINF)*RHOINF/ALPHA/MU

          OPEN(20,FILE="xcoord.data",STATUS='UNKNOWN')
```

```
      DO I = 1, N
           ETA(I) = DX*(I-1)
           X(I) = ETA(I)*Y/(RA**0.5)
           WRITE(20, FMT=160) X(I)
          ENDDO

          READ(40,FMT=150) (F(I), I=1,N-1)
          READ(50,FMT=150) (FPRIME(I), I=1,N-1)

c         WRITE(*,*) (FPRIME(I), I=1,N-1)

          OPEN(70,FILE='velocity1du.data',STATUS='UNKNOWN')
          OPEN(80,FILE='velocity1dv.data',STATUS='UNKNOWN')
          OPEN(90,FILE='temp1d.data',STATUS='UNKNOWN')
          OPEN(30,FILE='density.data',STATUS='UNKNOWN')

          DO I=1,N
           U(I) = 0.5*(ALPHA*RHOINF*g*B*K*(TW-TINF)/MU/Y)**0.5
     #       * (ETA(I)*FPRIME(I)-F(I))
           WRITE(70,FMT=150) U(I)
           V(I) = (RHOINF*g*B*(TW-TINF)*K/MU) * FPRIME(I)
        WRITE(80,FMT=150) V(I)
C         calculate temperatures too
           TEMP1D(I) = FPRIME(I)*(TW-TINF)+TINF
           WRITE(90,FMT=150) TEMP1D(I)

C         Calculate Densities
           DENSITY(I) = RHOINF * (1.D0 - B * (TEMP1D(I) - TINF))
           WRITE(30,FMT=150) DENSITY(I)

          ENDDO



          CLOSE(20)
          CLOSE(30)
          CLOSE(40)
          CLOSE(50)
          CLOSE(70)
          CLOSE(80)
          CLOSE(90)

          RETURN

          END
```

REFERENCES

Abramov, O., and D. A. Kring (2005), Impact-induced hydrothermal activity on early Mars, *J. Geophys. Res., 110*, E12S09, doi:10.1029/2005JE002453.

Abramov, O., and D. A. Kring (2004), Numerical modeling of an impact induced hydrothermal system at the Sudbury crater, *J. Geophys. Res., 109*, E10007, doi:10.1029/2003JE002213.

Baker, V. R. (2001), Water and the Martian landscape, *Nature, 412*, 228-236.

Baker, V. R., and D. J. Milton (1974), Erosion by catastrophic floods on Mars and Earth, *Icarus, 23*, 27– 41.

Baker, E. T., and C. R. German (2004), On the global distribution of hydrothermal vent fields, in *Mid-Ocean Ridges: Hydrothermal Interactions Between the Lithosphere and Oceans, Geophys. Monogr. Ser.,* vol. 148, edited by C. R. German, J. Lin, and L. M. Parson, pp. 245–266, AGU, Washington, D. C.

Baker, E. T. (2007), Hydrothermal cooling of midocean ridge axes: Do measured and modeled heat fluxes agree?, *Earth and Planetary Science Letters, 263*, 140–150.

Baross, J.A. and S.E. Hoffman (1985), Submarine hydrothermal vents and associated gradient environments as sites for the origin and evolution of life, *Origins of Life, 15*, 327-345.

Benjamin, S.B. (2004), Hydrothermal activity on the flanks of a fast-spreading ridge: Mineral deposits and sedimentary features recently discovered on East Pacific Rise abyssal hills, M.S. thesis, University of California, Santa Barbara, CA.

Bejan, A. (1995), *Convection Heat Transfer,* 2nd ed., 639 p., Wiley, New York.

Bischoff, J. L. and W. E. Seyfried (1978), Hydrothermal chemistry of seawater from 25° to 350 °C, *American Journal of Science, 278*, 838-860.

Bleacher J. E., R. Greeley, D. A. Williams, S. R. Cave, G. Neukum (2007), Trends in effusive style at the Tharsis Montes, Mars, and implications for the development of the Tharsis province, *J. Geophys. Res., 112*, E09005, doi:10.1029/2006JE002873.

Brakenridge, G. Robert, Horton E. Newsom, and Victor R. Baker (1985), Ancient hot springs on Mars: Origins and paleoenvironmental significance of small Marian valleys, *Geology, 13*, p. 859-862

Brass, G. W. (1980), Stability of brines on Mars, *Icarus, 42*, 20-28.

Burt, D.M. and L.P. Knauth (2003), Electrically conducting Ca-rich brines, rather than water, expected in the Martian subsurface, *J. Geophys. Res., 108*, 8026, doi: 10.1029/2002JE002233.

Carlsaw, H. S. and J. C. Jaeger (1959), *Conduction of Heat in Solids*, 2nd ed., 510 p., Oxford University Press, Oxford.

Carr, M. H. (1979), Formation of Martian flood features by release of water from confined aquifers, *J. Geophys. Res., 84*, 2995– 3007.

Cheng, P. and W. Minkowycz (1977), Free convection about a vertical flat plate embedded in a porous medium with application to heat transfer from a dike, *J. Geophys. Res., 82*, 2040-2044.

Cherkaoui, A. S. M., W. S. D. Wilcock, R. A. Dunn, and D. R. Toomey (2003), A numerical model of hydrothermal cooling and crustal accretion at a fast spreading mid-ocean ridge, *Geochem. Geophys. Geosyst., 4*, 8616, doi:10.1029/2001GC000215.

Christeson, G., L. G. M. Purdy, and G. J. Fryer (1992), Structure of young upper crust at the East Pacific Rise near 9° 30′ N, *Geophys. Res. Lett., 19*, 1045–1048.

Christeson, G. L., K. D. McIntosh, and J. A. Karson (2007), Inconsistent correlation of seismic layer 2a and lava layer thickness in oceanic crust, *Nature, 445*, 418–421.

Christeson, G. L., G. M. Purdy, and G. J. Fryer (1994), Seismic constraints on shallow crustal emplacement processes at the fast spreading East Pacific Rise, *J. Geophys. Res.*, *99*, 17,957–17,973.

Clifford, S.M. (1993), A model for the hydrologic and climatic behavior of water on Mars, *J. Geophys. Res., 98*, 10,973-11,016.

Cloy, G. D. (1984), Radiation-dominated snowmelt on Mars. In *MECA Workshop on Water on Mars,* pp. 15-16.

Dunn, R., D. R. Toomey, and S. C. Solomon (2000), Three-dimensional seismic structure and physical properties of the crust and shallow mantle beneath the East Pacific Rise at 9° 30′ N, *J. Geophys. Res., 105*, 23,537-23,555.

Edmond, J. M., K. L. Von Damm, R. E. McDuff, and C. I. Measures (1982), Chemistry of hot springs on the East Pacific Rise and their effluent dispersal, *Nature, 297*, 187-191.

Edmond, J. M., C. Measures, R. E. McDuff, L. H. Chan, R. Collier, B. Grant, L. I. Gordon, and J. B. Corliss (1979), Ridge crest hydrothermal activity and the balances

of the major and minor elements in the ocean: The Galapagos data, *Earth Planet. Sci. Lett., 46*, 1–18.

Edmond, J.M., A. C. Campbell, M. R. Palmer, C. R. German, G.P. Klinkhammer, H. N. Edmonds, H. Elderfield, G. Thompson, and P. A. Rona (1995), Time series studies of vent fluids from the TAG and MARK sites (1986, 1990) Mid-Atlantic Ridge and a mechanism for Cu/Zn zonation in massive sulphide ore bodies, in *Hydrothermal Vents and Processes, Geol. Soc. Spec. Publ.*, vol. *87*, pp. 77–86.

Elderfield, H. and A. Schultz (1996), Mid-ocean ridge hydrothermal fluxes and the chemical composition of the ocean, *Ann. Rev. Earth Planet. Sci., 24*, 191-224.

Fouquet, Y., K. Henry, R. Knott, and P. Cambon (1998), Geochemical section of the TAG hydrothermal mound, *Proceedings of the Ocean Drilling Program*, *Scientific Results, 158*, 363-387.

Fowler, C. M. R. (2005), *The Solid Earth*, 2nd ed., 685 pp., Cambridge Univ. Press, New York.

Francheteau, J., R. Armijo, J. L. Cheminee, R. Hekinian, P. Lonsdale, and N. Blum (1992), Dyke complex of the East Pacific Rise exposed on the walls of Hess Deep and the structure of the upper oceanic crust, *Earth Planet. Sci. Lett., 111*, 109–121.

Germanovich, L. N., R. P. Lowell, D. K. Astakhov (2001), Temperature-dependent permeability and bifurcations in hydrothermal flow, *J. Geophys. Res., 106*, 473-495.

Germanovich, L. N., R. P. Lowell, D. K. Astakhov (2000), Stress-dependent permeability and the formation of seafloor event plumes, *J. Geophys. Res., 105*, 8341-8354.

Gulick, V. (2001), Origin of the valley networks on Mars: a hydrological perspective, *Geomorphology, 37*, 241-268.

Gulick, V. (1998), Magmatic intrusions and a hydrothermal origin for fluvial valleys on Mars, *J. Geophys. Res.*, *103*, 19365-19387.

Harding, A. J., G. M. Kent, and J. A. Orcutt (1993), A multichannel seismic investigation of upper oceanic crust at 9°N on the East Pacific Rise: Implications for crustal accretion, *J. Geophys. Res., 98*, 13,925–13,944.

Hartmann, W. K. (2001), Martian seeps and their relation to youthful geothermal activity: *Space Science Reviews, 96*, 405-410.

Haymon, R. M., K. C. Macdonald, S. B. Benjamin, and C. J. Ehrhardt (2005), Manifestations of hydrothermal discharge from young abyssal hills on the fast-spreading East Pacific Rise flank, *Geology*; *33*, no. 2, 153-156.

Humphris, S. E., and M. K. Tivey (2000), A synthesis of geological and geochemical investigations of the TAG hydrothermal fluid: Insights into fluid flow and mixing processes in a hydrothermal system, in *Ophiolites and Oceanic Crust: New Insights From Field Studies and the Ocean Drilling Program*, Boulder, CO, Geol. Soc. of Am. Spec. Pap. 349, pp. 213–235.

Jakosky, B. and R. Phillips (2001), Mars' volatile and climate history. *Nature, 412*, 237-244.

James, R. H., and H. Elderfield (1996), Chemistry of oreforming fluids and mineral formation rates in an active hydrothermal sulfide deposit on the Mid-Atlantic Ridge, *Geology, 24*, 1147–1150.

Kappus, M. E., A. J. Harding, and J. A. Orcutt (1995), A baseline for upper crustal velocity variations along the East Pacific Rise at 13°N, *J. Geophys. Res., 100*, 6143–6161.

Knauth, L.P. and D.M. Burt (2002), Eutectic brines on Mars: Origin and possible relation to young seepage features, *Icarus, 158*, 267-271.

Lewis, K.C. (2007), Numerical modeling of two-phase flow in the sodium chloride-water system with applications to seafloor hydrothermal systems, Ph.D. thesis, Georgia Institute of Technology, Atlanta, GA.

Lowell, R.P., S. Gosnell, and Y. Yang (2007), Numerical simulations of single-pass hydrothermal convection at mid-ocean ridges: Effects of the extrusive layer and temperature-dependent permeability, *Geochem. Geophys. Geosys., 8*, Q10011, doi:10.1029/2007GC001653.

Lowell, R. P., Y. Yao, and L. N. Germanovich (2003), Anhydrite precipitation and the relationship between focused and diffuse flow in seafloor hydrothermal systems, *J. Geophys. Res., 108*, 2424, doi:10.1029/2002JB002371.

Malin, M., and K. Edgett (2000), Evidence for recent groundwater seepage and surface runoff on Mars, *Science, 288*, 2330-2335.

Manning, C. E., C. J. MacLeod, and P. E. Weston (2000), Lower-crustal cracking front at fast-spreading ridges: Evidence from the East Pacific Rise and the Oman ophiolite, in *Ophiolites and Oceanic Crust: New Insights from Field Studies and the Ocean Drilling Program*, Boulder, CO, Geological Society of America Special Paper 349, p. 261-272.

Max, M.D. and S.M. Clifford (2001), Initiation of Martian outflow channels: Related to the dissociation of gas hydrate?, *Geophys. Res. Lett., 28*, 1787-1790.

McKenzie, D., and Nimmo, F. (1999), The generation of martian floods by the melting of

ground ice above dykes, *Nature*, *397*, 231-233.

Mouginis-Mark, P. J. (1990), Recent water release in the Tharsis region of Mars, *Icarus, 84*, 362-373.

NASA (2008), NASA Spacecraft Confirms Martian Water, Mission Extended, *NASA Press Release*, 08-195, Media contacts: G. Webster, S. Hammond, D. Brown.

NASA (2006), NASA Images Suggest Water Still Flows in Brief Spurts on Mars. *NASA Press Release*, 06-362, Media contacts: D. Brown, E. Hupp, and G. Webster.

Nehlig, P. and T. Juteau (1988), Flow porosities, permeabilities and preliminary data on fluid inclusions and fossil thermal gradients in the crustal sequence of the Sumail ophiolite (Oman), *Tectonophysics, 151*, 199-221.

Newsom, H. E., Brittelle, G. E., Hibbitts, C. A., Crossey, L. J., and Kudo, A. M. (1996), Impact crater lakes on Mars, *J. Geophys. Res.-Planets*, *101*, no. E6, 14951-14955.

Ogawa, Y., Y. Yamagishi, and K. Kurita (2003), Evaluation of melting process of the permafrost on Mars: Its implication for surface features, *Journal of Geophysical Research-Planets*, *108*, no. E4, 8046, doi:10.1029/2002JE001886.

Pascoe, A. R., and J. R. Cann (1995), Modeling diffuse hydrothermal flow in black smoker vent fields, in *Hydrothermal Vents and Processes*, edited by L. M. Walker and C. L. Dixon, Geol. Soc. Spec. Publ., 87, pp. 159–173.

Plaut, J.J. et al. (2007), Subsurface radar sounding of the South Pole layered deposits of Mars, *Science, 316*, doi: 10.1126/science.1139672

Pollack, J. B., J. F. Kasting, S. M. Richardson, and K. Poltakoff (1987), The case for a wet, warm climate on early Mars, *Icarus, 39*, 88-110.

Rathbun, J. and S. Squyres (2002), Hydrothermal systems associated with Martian impact craters, *Icarus, 157*, p. 362-372.

Ramondenc, P., L. N. Germanovich, and R. P. Lowell (2008), Modeling hydrothermal response to earthquakes at oceanic spreading centers in, *Magma to Microbe*: *Modeling Hydrothermal Processes at Seafloor Spreading Centers*, *Geophys. Monogr. Ser.*, v. *177*, ed. by R.P. Lowell, J.S. Seewald, A. Metaxas, and M.R. Perfit, p. xxx, Amer. Geophys. Union, Washington, DC (in press).

Ramondenc, P., L. N. Germanovich, K. L. Von Damm, and R. P. Lowell (2006), The first measurements of hydrothermal heat output at 9_500 N, East Pacific Rise, *Earth Planet. Sci. Lett., 245*, 487–497, doi:10.1016/j.epsl.2006.03.023.

Rodriguez, J.A.P., et. al.(2005), Control of impact crater fracture systems on subsurface hydrology, ground subsidence, and collapse, Mars, *J. Geophys. Res., 110*, E06003, doi:10.1029/2004JE002365.

Rodriguez, J. A. P., J. Kargel, D. A. Crown, L. F. Bleamaster III, K. L. Tanaka, V. Baker, H. Miyamoto, J. M. Dohm, S. Sasaki, and G. Komatsu (2006), Headward growth of chasmata by volatile outbursts, collapse, and drainage: Evidence from Ganges chaos, Mars, *Geophys. Res. Lett., 33*, L18203, doi:10.1029/2006GL026275.

Rona, P. A. and D. A. Trivett (1992), Discrete and diffuse heat transfer at ASHES vent field, Axial Volcano, Juan de Fuca Ridge, *Earth Planet. Sci. Lett., 109,* 57-71.

Scheirer, D. S., T. M. Shank, and D. J. Fornari (2006), Temperature variations at diffuse and focused flow hydrothermal vent sites along the northern East Pacific Rise, *Geochem. Geophys. Geosyst., 7*, Q03002, doi:10.1029/2005GC001094.

Schultz, A., J. M. Delaney, and R. E. McDuff (1992), On the partitioning of heat flux between diffuse and point source venting, *J. Geophys. Res., 97*, 12,229–12,314.

Schultz, P. H. (1985), The Martian atmosphere before and after the Argyre impact, In *MECA Workshop on the Evolution of the Martian Atmosphere,* pp. 22-23.

Sears, D.W.G and J.D. Crittendon (2005), On laboratory simulation and the temperature dependence of the evaporation rate on Mars, *Geophys. Res. Lett., 32*, L23203, doi: 10.1029/2005GL024154.

Sears, D.W.G and S. R. Moore (2005), On laboratory simulation and the evaporation rate of water on Mars, *Geophys. Res. Lett., 32*, L16202, doi:10.1029/2005GL023443.

Spiess, F. N., et al. (1980), East Pacific Rise: Hot springs and geophysical experiments, *Science, 207*, 1421–1433.

Squyres, S., D. Wilhelms, and A. Moosman (1987), Large-Scale Volcano-Ground Ice Interactions on Mars, *Icarus, 70*, 385-408.

Stein, C.A., and S. Stein (1994), Constraints on hydrothermal heat flux through the oceanic lithosphere from global heat flow. *J. Geophys. Res., 99*, 3081–3095.

Tivey, M. K., R. A. Mills, and D. A. H. Teagle (1998) Temperature and salinity of fluid inclusions in anhydrite as indicators of seawater entrainment and heating in the TAG active mound, *Proceedings of the Ocean Drilling Program. Scientific Results*, *158*, 179-190.

Trumble, M. E., J. E. Bleacher, A. de Wet, D. J. Merritts, and W. B. Garry (2008), Geomorphologic mapping and characterization of channel networks on the Tharsis Montes, Mars, *39th Lunar and Planetary Science Conference LPI*, *LPI Contribution* No. *1391*, p.1698.

van Everdingen, D. A. (1995), Fracture characteristics of the Sheeted Dike Complex, Troodos ophiolite, Cyprus: Implications for permeability of oceanic crust, *J. Geophys. Res.*, *100*, 19,957–19,972.

Vera, E. E., and J. B. Diebold (1994), Seismic imaging of oceanic layer 2A between 9°30′N and 10°N on the East Pacific Rise from two-ship wide-aperture profiles, *J. Geophys. Res.*, *99*, 3031–3041.

Veirs, S. R., R. E. McDuff, and F. R. Stahr (2006), Magnitude and variance of near-bottom horizontal heat flux at the Main Endeavour hydrothermal vent field, *Geochem. Geophys. Geosys., 7*, Q02004, doi:10.1029/2005GC000952.

Von Damm, K. L., and M. D. Lilley (2004), Diffuse flow hydrothermal fluids from 9° 50′ N East Pacific Rise: Origin, evolution and biogeochemical controls, in *The Subsurface Biosphere at Mid-Ocean Ridges, Geophys. Monogr. Ser.*, vol. 144, edited by W. S. D. Wilcock et al., pp. 245–268, AGU, Washington, D. C.

Von Damm, K. L., S. E. Oosting, R. Kozlowski, L. G. Buttermore, D. C. Colodner, H. N. Edmonds, J. M. Edmond and J. M. Grebmeier (1995), Evolution of East Pacific Rise hydrothermal vent fluids following a volcanic eruption, *Nature, 375*, 47 – 50.

Von Damm, K. L. (1990), Seafloor hydrothermal activity: black smoker chemistry and chimneys, *Annual Review of Earth and Planetary Sciences, 18*, 173-204.

Voss, C. I. (1984), SUTRA, U.S. Geol. Surv. Water Resour. Inv. Rep. 84-4369.

Wilcock, W. S. D. and A. McNabb (1996), Estimates of crustal permeability on the Endeavour segment of the Juan de Fuca mid-ocean ridge, *Earth and Planetary Science Letters, 138*, 83-91.

Wolery, T. J. and N. H. Sleep (1976), Hydrothermal circulation and geochemical flux at mid-ocean ridges, *J. Geol., 84*, 249-275.